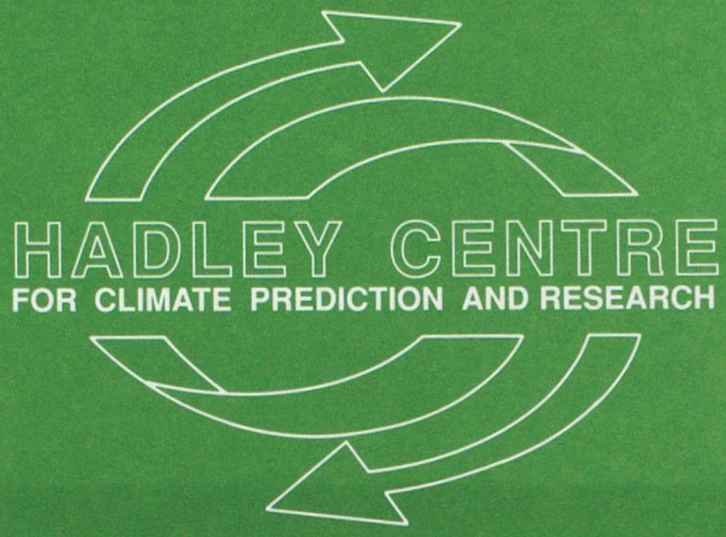

The temporal evolution of Equatorial Currents in the Indian Ocean.

by

D. L. T. Anderson, D. J. Carrington, R. A. Corry and C. Gordon

CRTN 23 February 1992

CLIMATE RESEARCH TECHNICAL NOTE

Hadley Centre
Meteorological Office
London Road
Bracknell
Berkshire RG12 2SY

CLIMATE RESEARCH TECHNICAL NOTE NO. 23

THE TEMPORAL EVOLUTION OF EQUATORIAL CURRENTS IN THE INDIAN OCEAN

by

D L T Anderson, D J Carrington, R Corry and C Gordon

Hadley Centre for Climate Prediction and Research
Meteorological Office
London Road
Bracknell
Berkshire RG12 2SY
U. K.

NOTE: This paper has not been published. Permission to quote from it should be obtained from the Director of the Hadley Centre.

Abstract

A General Circulation Model of the Indian Ocean is used to analyse the seasonal cycle of equatorial currents in response to a realistic wind forcing providing a comprehensive simulation of currents in the upper few hundred meters. Model results compare favourably with the known surface currents and with some aspects of the limited subsurface observations. However, the notion that the undercurrent is stronger and larger-lived in the western ocean is not confirmed by the model results. A conventional undercurrent is present all along the equator in January–March. A 'reverse' undercurrent is present in July and August over most of the basin suggesting that it is not difficult to have latitudually confined westward jets on the equator, contrary to some undercurrent theories. There is a marked semi-annual cycle in currents beneath the undercurrent, although deeper currents are of smaller amplitude than observed and deep jets are not well-modelled. The semi-annual cycle is associated with a westward propagating second mode Rossby wave, clearly seen at 600m.

1. Introduction

Over the tropical Atlantic and Pacific oceans, westward tradewinds prevail and the ocean surface flow has a mean westward component. Water accumulates near the western boundaries, sea level stands higher there and consequently a pressure gradient force toward the east exists in the upper layers. The westward wind also drives a poleward Ekman flow in the surface layers of both hemispheres, creating a divergence near the equator which is compensated by upwelling. The upwelled water is in turn replaced by a meridionally-convergent flow in the thermocline, in geostrophic balance with the eastward pressure gradient force. Near the equator, this geostrophic balance breaks down, and a jet-like eastward current in the thermocline arises; the pressure gradient is balanced not by Coriolis force due to meridional velocity but by vertical diffusion or vertical advection of momentum involving the zonal flow in the jet. This jet is the equatorial undercurrent, a major permanent feature of the Atlantic and Pacific circulations.

By contrast, the winds in the tropical Indian Ocean and thus the ocean circulation, are profoundly different. The zonal wind is eastward in the mean, the opposite of the other oceans. Because of nonlinear processes, to be discussed later, the response to an eastward wind is not the reverse of that to a westward wind, so we can expect the Indian Ocean currents to behave differently from those in the Atlantic and Pacific. Further the winds over the Indian Ocean have a strong semi-annual variation. The oceanic response to such a strongly time dependent forcing is very different from that to the nearly steady easterlies of the Atlantic or Pacific.

There are three aspects of the equatorial Indian Ocean circulation which will be considered here: the eastward equatorial surface jet, the equatorial undercurrent, and the deep jets which exist below the thermocline. The first of these was well documented from historical ship drift data by Wyrtki (1973). The jet appears to be strongest in the central ocean, which is probably a result of two effects: firstly the equatorial eastward winds of

the monsoon transitions begin to blow sooner and stronger over the central and eastern ocean, and secondly, near the eastern boundary the direct acceleration of the jet by the wind is soon offset by the influence of the coast (reflected Rossby wave), so that over a one month average the current appears less. Vertical profiles of velocity near Gan (73°E) (Knox (1976)) and also at 55°E (Leetmaa and Stommel (1980)) show the twice-yearly spin-up of this current as do currents inferred from equatorial drifting buoys (Luyten *et al.*, (1980), Cresswell *et al.*, (1981)) which often move eastward with the jet for substantial distances of up to 4000 km at speeds averaging more than 50 cm/s.

The equatorial undercurrent (UC) of the Indian Ocean was known from the work of the International Indian Ocean Expedition (IIOE) to vary with the monsoons. Taft and Knauss (1967) showed surveys in opposite seasons of the year. At the end of the northeast monsoon the undercurrent appeared to be an ocean-wide feature, like its Atlantic and Pacific counterparts, but not during the fall-to-late southwest monsoon.[1] Swallow (1964) reported a stronger, longer-lasting undercurrent, using data from the western part of the ocean and a different year. Leetmaa and Stommel (1980) (hereafter L-S), from 2 years of springtime (February to June) cross-equatorial profiles near 55°E, found an eastward subsurface current from February to May. In May and June this shifted south to merge with an eastward subsurface countercurrent near 3°S. On the other hand the profiles near Gan show a conventional undercurrent in only two of the three years sampled. It is present in 1973, absent in 1974, and weakly present in 1975 (Knox and McPhaden (1980)). This and the above cited references have been interpreted as giving the impression that the undercurrent is a stronger, longer-lived flow in the western ocean than in the center or east. The results of this study, however, suggest that this may not be a correct interpretation.

In 1976, Luyten and Swallow (1976) published full-depth current profiles from the Indian Ocean equator showing that the vertical structure was far more complex than previously suspected. There was not just one undercurrent but several deep flows. These

[1] *Since the Taft and Knauss surveys are not easy to obtain, some of their diagrams showing N-S transects of velocity are included in Appendix 1.*

were weaker than the undercurrent with typical strengths of 15 cm/s. These zonal jets were equatorially trapped but of long zonal scale. The month-long 1976 observations did not resolve their (long) period, but moored records show, for example, a strong semiannual variation at 700 m (Luyten and Roemmich, (1982) hereafter denoted L–R). These deep jets have been further observed in the Indian Ocean during FGGE (Ponte and Luyten (1990)).

In this paper we examine a multi-level model of the Indian Ocean circulation, driven by realistic winds, to verify the model against what few observations there are and to extend our knowledge of the seasonal response of the subsurface flow, mainly of the undercurrent but of the deeper flows also where the model can adequately simulate them. In section 2, a review of theories and models of the undercurrent and some aspects of the deep jets is given. The model used in this study is described in section 3 and results are given in section 4.

2. Theoretical considerations

In the linear case, the steady bounded ocean response to a uniform zonal wind is a pressure gradient balancing the wind stress and no flow at all, neither in the surface layer nor at any depth; there is no undercurrent nor any deep jets. This constraint can be broken if there is vertical mixing or vertical mass exchange. If the ocean is represented as layers or vertical normal modes then a term such as Q in the "continuity equation"

$$h_t + H\,(u_x + v_y) = Q \tag{2.1}$$

is sufficient to prevent a perfect balance being established between the pressure gradient and the wind and there must then be motion. An equation of the form (2.1) is used in many tropical problems, and different interpretations can be given to Q. In the model of McCreary (1981) Q represents a parameterisation of vertical mixing. An alternative interpretation is that it represents a mass exchange between layers.

In the model of Cane (1980) (to be discussed below) the upper layer is always of fixed depth regardless of dynamics, so there must be an implicit exchange of mass between the

two layers. In the model of Philander and Pacanowski (1980), also discussed below, there is vertical mixing which moves heat around and so alters the mass of fluid between isopycnals. More recently, it has been argued that the deep jets can be driven by thermohaline processes, which may be modelled by including a mass source term in a continuity equation akin to (2.1) (Kawase (1987)). In all cases then, the balance between the pressure gradient and wind stress can never become fully established and so undercurrents and possibly deep jets can form.

Cane (1980) has modelled the spin up, steady state, and spin down of equatorial currents driven by eastward and westward wind stresses. The model is a $2\frac{1}{2}$-layer system, but the upper two layers have no density contrast, so there is only one baroclinic mode. The top layer serves as a region over which the wind stress is uniformly distributed as a body force allowing the development of a shear across the upper 2 layers, even though their density is uniform. The model is nonlinear, and the key process which this permits is vertical advection of zonal momentum (wu_z), making the response to eastward and westward winds asymmetrical. The main results of Cane's studies are that for <u>both</u> westward and eastward winds the steady state total transport is eastward.

Cane considered responses to (i) switch-on of westward winds, (ii) switch-on of eastward winds, (iii) switch-off of westward winds, and (iv) switch-off of eastward winds. For a linear system, responses to (i) and (ii) would just be opposite in sign, as would responses to (iii) and (iv). For the nonlinear case, however, they are different. Before the effects of coasts have had time to propagate to the point of interest in the interior, there is no zonal pressure gradient, and the flow responds directly to the wind. Eastward winds put eastward momentum into the forced layer, and this is advected downward by the vertical velocity which results from Ekman convergence, in addition to being diffused downward by friction. For westward winds, however, the Ekman flow is divergent and the vertical velocity is upward, so advection opposes diffusion and the acceleration of the deeper layers is slower. This is the basic nonlinear asymmetry, and we see that it can account for the

rapidity of response to eastward winds, in both of the active layers of the model. As time progresses, Kelvin (Rossby) waves originating at the western (eastern) boundary propagate to interior points and eventually lead to the establishment of a steady pressure gradient. For westward winds this effect overcomes the westward flow in the middle layer which was initially forced by the wind, and a conventional undercurrent results. For eastward winds the flow in both layers continues to be eastward. It decreases in the middle layer as the pressure gradient is set up, but in the Cane model the pressure gradient never becomes strong enough to reverse the flow at undercurrent level.

The responses (iii) and (iv) to cessation of winds allow pre-existing steady circulations to change and relax. Again the early stages take place before the alterations of zonal pressure gradients due to waves. For switch-off of westward winds the loss of westward momentum of the surface wind leads to reversal of the surface layer flow, but at the middle level, where the flow is already nearly in balance with the pressure gradient, change is initially slight. When eastward winds are turned off, however, the downward advection of eastward momentum which maintained eastward middle-level flow against the pressure gradient is stopped and both surface and middle layers decelerate rapidly. A refinement of this process, in which the eastward winds are not switched off but are changed to northward winds, shifts the middle-level current system upwind and brings a band of westward flow to the equator, i.e. a reversal rather than just a deceleration. Cane applies these results to a series of observations by Knox at Gan (73°E on the Equator) when an undercurrent was observed in 1972 but not in 1973 and argues that this could account for the observed behaviour at Gan in January/February 1974, when both the surface and subsurface flow changed rapidly from eastward to westward.

An alternative explanation to account for the lack of an eastward undercurrent at Gan in early 1974 is that the autumn round of eastward winds relaxed in October 1972 whereas in 1973 they lasted until December. Thus in early 1974 there had not been enough time for an undercurrent to arise as a response to westward winds before the onset of the

spring 1974 round of eastward winds. Cane also notes that in the year of Swallow's (1964) undercurrent observations the preceeding eastward winds had died earlier than in the year of Taft and Knauss' (1967) measurements, consistent with Swallow having observed a longer-lasting undercurrent at comparable longitudes.

Philander and Pacanowski (1980) have also modelled flow in response to switched-on winds using a GCM model. They support Cane's results that the nonlinear effects of the vertical circulation induced by the wind are important. In the early stages, the eastward surface flow in response to eastward winds is strengthened relative to the linear case while that of a westward flow in response to westward winds is reduced. The thermocline flow in response to an eastward wind is to the east but it is weaker than in the linear case and weaker than the (eastward) flow in response to a westward wind. It takes in the order of 150 days to reach equilibrium but (see Fig. 7, Philander and Pacanowski (1980)) this is very much a function of longitude and whether winds are eastward or westward. Unlike in the case of Cane, however, the time for boundary effects to be important is altered by mean currents: for eastward flow they find that the time for Rossby waves to propagate from the eastern boundary is increased although the time for Kelvin waves to propagate from the western boundary is not altered.

Steady currents in response to eastward and westward winds are also different. The flow is shallower in the case of eastward winds but in both cases the subsurface flow is primarily eastward along the equator with return flows to the north and south. (See Fig. 12, Philander and Pacanowski (1980)).

When a westward wind is turned off (somewhat like turning on a eastward wind), there is a surge in the undercurrent which rises to the surface giving eastward flow there. When an eastward wind relaxes, the pressure gradient reverses the surface flow very quickly and the eastward undercurrent is replaced by an accelerating westward current. (In Cane, the eastward undercurrent decelerates but over most of the basin it does not reverse: in fact it subsequently surges as a consequence of a reversed pressure gradient associated with wave

propagation.)

The time dependence of the flow beneath the thermocline, and in particular the extent to which the semiannual periodicity, so strong near the surface, penetrates the deep ocean has also been examined. Initially it was thought that the deep jets observed by Luyten and Swallow were wind driven and Wunsch (1977) used an inviscid linear model to show a mechanism by which vertically structured, semiannual, equatorially trapped flow could arise. He assumed an unbounded ocean (in depth as well as horizontal) forced from above at semiannual period and a single zonal wavenumber. His results exhibit numerous vertical zonal flow reversals.

When the finite width of the ocean is taken into account, McCreary (1984) showed that coasts play an important role in reflecting energy into the deep ocean and that the Wunsch mechanism cannot be correct. McCreary used a linear model with an imposed stratification. His results were questioned by Gent and Luyten (1985) who argued that energy in beams could not penetrate the sharp equatorial thermocline but would be reflected from it. This result was in turn refuted by Rothstein *et al.* (1985) who showed that beams could propagate through realistic thermoclines with very little reflection. According to Rothstein *et al.* (1988) a more serious impediment to deep penetration was critical layer absorption of Kelvin wave energy. It appears that Rossby waves are not subject to this absorption so that Rossby beams can penetrate the deep ocean. The beams generated in McCreary's model are not vertically propagating (at a fixed longitude) whereas the observations (in at least some oceans) show that the deep jets are associated with vertical propagation. There is therefore some uncertainty as to whether wind forcing can be the mechanism for exciting these deep jets.

While all the above theory is a useful framework for understanding equatorial dynamics, it has been conducted using models which are either too simple (containing only subsets of the physics) or use wind forcing fields which are grossly over-simplified. A more coherent test would be to run a realistic model with realistic winds. The model results

should then be compared with observations. Unfortunately, subsurface observations in the Indian Ocean are incredibly scanty. They are summarised in table 1.

The ocean is a forced system, so the forcing fields are of primary importance. Unfortunately, the wind field is only imperfectly known. Existing wind data sets are

(i) the climatological sets of Hellerman and Rosenstein (1983) and Han and Lee (1983)

(ii) the 1954 to 1976 data set of Cadet and Diehl (1984)

(iii) the 1977 to 1990 FSU data set (Legler *et al.*, 1989)

(iv) data sets from operational weather centres such as ECMWF, NMC and the U.K. Met. Office.

Unfortunately there are substantial differences between the wind data sets, and these differences can be sufficiently large to give rise to differences in current strengths comparable to the interannual differences. In this paper we will consider a seasonal cycle integration forced by the Hellerman and Rosenstein winds. In a subsequent paper (Anderson and Carrington (1992)) we will consider specific integrations using the UKMO and ECMWF winds.

3. Description of the model

The primitive equations are solved numerically using the model of Cox (1984) based on the finite–differencing method discussed in Bryan (1969), but with the vertical eddy diffusion scheme of Pacanowski and Philander (1981). The vertical eddy viscosity is assigned a minimum value of 10 cm^2s^{-1} in the upper 10m (i.e. in the first layer) of the model to take account of mixing by high frequency winds not present in the model forcing. There are 16 levels in the vertical in a constant depth ocean of 4000m. The upper 40m have 10m resolution. The model domain extends from 35°E to 125°E, and from 36°S to 27°N. The geometry is fairly realistic (except near Southern Africa where the model coastline lies along the 35°E line of longitude). The north-south grid spacing is 0.3° at the equator, increasing poleward to a maximum of 1° while the east-west spacing varies from 0.5° in the west to 1.5° in the east. The southern boundary is open; all other boundaries are

closed. The coefficient of diffusion in the meridional direction is high near the southern boundary ($3\times10^4 m^2 s^{-1}$) decreasing to a constant value of $2\times10^3 m^2 s^{-1}$ more than 5 grid-points points from the boundary, while that in the zonal direction has a constant value of $2\times10^3 \mathrm{m}^2\mathrm{s}^{-1}$. The horizontal eddy viscosity is 10^4 $\mathrm{m}^2 s^{-1}$ at a resolution of 1.5°, decreasing linearly with the zonal spacing to a minimum of $3.3\times10^3 m^2 s^{-1}$.

The model is forced using the seasonally varying stresses calculated by Hellerman and Rosenstein (1983). The heat flux is parameterised as

$$Q = Q_c + \lambda(T_c - T)$$

where Q_c is the climatological net surface heat flux interpolated in time from the monthly-mean values of Esbensen and Kushnir (1981), T_c is the monthly-mean sea surface temperature (SST) climatology and T is the temperature of the model surface layer. This formulation is equivalent to that of Haney (1971). All components of the heat flux except for the solar radiation are absorbed at the first level. The solar flux is allowed to penetrate below the top model layer; its attenuation with depth follows the scheme of Paulson and Simpson (1977) with constant Jerlov optical water-type 1B.

The additional term $\lambda(T_c - T)$ is a negative feedback term to constrain the surface temperature. If the heat flux Q_c was 'correct', the stress correct and the model formulation and initial conditions perfect, then there would be no need for this term. However, there is no other negative feedback in the model (except on the southern boundary), and if, for example, the heat flux Q_c was too high or the model poorly formulated so that the vertical redistribution of heat was inadequate, then surface temperatures could continue to rise if it were omitted. The term $\lambda(T_c - T)$ term provides a check on this, relaxing the modelled sea surface temperature back to its climatological value. Note that errors in the wind stress climatology can also give rise to an anomalous heat flux as the SST is affected by advection and upwelling which are related to wind stress. The value used for λ is 35 $\mathrm{Wm}^{-2}K^{-1}$, which corresponds to a damping time of 60 days for a 50m thick layer.

The precipitation minus evaporation in the seasonal cycle integration is treated in a

similar way to the heat flux

$$P - E = (P_c - E_c) + \lambda_s(S_c - S)$$

The monthly mean precipitation climatology, P_c, is taken from Jaeger (1976). The evaporation, E_c, is calculated from the Esbensen and Kushnir latent heating, with λ_s taken to give the same feedback timescale as for temperature. The climatological salinity S_c is from Levitus (1982). There is no physical justification for this feedback in the case of salinity forcing. The anomalous heat flux term $\lambda(T_c - T)$ and precipitation minus evaporation term $\lambda_s(S_c - S)$ are of interest since they can point out gross errors in Q_c, S_c or $(P_c - E_c)$ or problems with the ocean model. They are discussed in Carrington (1990) but will not be considered in this paper.

The initial temperature and salinity data for the seasonal cycle integration were the Levitus data for September. The initial velocities were zero, and the calculation started in mid-September in a 360 day year. Since the ocean model used in this study has no bottom topography there are points where there are no Levitus data (i.e. where the ocean model is deeper than the real ocean). In such situations an average value was used based on neighbouring Levitus data at the same level. The model was run for four years and four months. Results discussed here are taken from the last full year of integration. The same model was used to study aspects of the seasonal cycle of the Somali current and some additional description of the model and non equatorial results are given to Anderson *et al.*, (1991).

4. Model Results

4.1 The surface flow

A prominent feature of the surface equatorial flow is the Wyrtki (or Yoshida) jet, a strong narrow eastward flow which, according to Wyrtki, is most pronounced in May and October/November and appears to be strongest in mid ocean. The temporal evolution of observed surface zonal velocity along the equator (derived from ship-drift measurements)

is shown in Fig. 1a from Reverdin (1987) which shows clearly the Wyrtki jet in May and October/November reaching monthly mean speeds of 80 cms^{-1}. Fig. 1a not only shows that the annual mean flow is eastwards over the Indian Ocean, particularly in the eastern half of the basin, but that there is an interesting strong westward flow over much of the equatorial region in February with a weaker westward flow occurring during the SW monsoon in the western half of the basin.

The model seasonal cycle of currents is shown in Fig. 1b for comparison. The westward flow in February at $\sim 60 cms^{-1}$ is comparable to the climatological values in fig. 1a, but is weaker than the currents observed by Leetmaa and Stommel (1980) when currents reach 80 cms^{-1} in 1975 and 100 cms^{-1} in 1976. The model Wyrtki jet is very strongly eastward from 60°E to 90°E in Spring and Autumn in good agreement with the observations, but the strength of the modelled Wyrtki jet at $120 cms^{-1}$ in May is significantly stronger than the observed strength based on ship-drift measurements. However at Gan 73°E, i.e. somewhat west of the maximum currents of Fig. 1a, Knox (1976) observed 'instantaneous' currents up to 1.3 ms^{-1}, with monthly-averaged currents in excess of 1 ms^{-1}. So the model strength may not be too unreasonable, although the Knox data do not represent a climatological average. Fig. 2b, c shows the spatial pattern of model currents in May and October at times close to the height of the Wyrtki jet, indicating that the current is indeed quite narrow.

The winds in the equatorial zone are primarily eastward so one would expect the surface currents to be primarily eastwards also. Only for a short time in the west are the winds westward (see Fig. 3) and hence a strong westward flow along the equator might not be expected. Yet Fig. 1b and 2a show that the modelled currents are strongly westward in February. The westward flow at this time is in good agreement with Fig. 1a which indicates currents of 60 cms^{-1}. L-S also find strong westward currents during the Spring period. Their published results do not include monthly averages, but westward velocities of 80 cms^{-1} do occur several times in February-March at 55°E. This westward flow is likely

to result from a relaxation of the eastward winds, inducing a surge, as well as from a local response to westward winds.

The data of L-S also indicate that the westward flow is more prevalent in the N.H. than in the S.H, in agreement with Fig. 2a. Not only is the westward flow centered north of the equator, it is much broader than the eastward flow of Fig. 2b, c, consistent with the results of Sec. 2. To give some idea of the seasonal changes in off-equatorial currents, Fig. 4a, b show the temporal variations in zonal velocities along north-south sections at 60°E and 80°E. Fig. 4a shows clearly the more confined nature of the eastward jets compared to the westward flow while Fig. 4b shows that although there is westward flow in February at 80°E, it is not primarily an equatorial phenomenum but more associated with the Sri Lankan current.

4.2 The Semi-annual response

As indicated in section 2, the semi-annual cycle, the dominant signal below the upper 200m, is best documented in the western part of the basin, so we will consider this region first. The model zonal velocity at 55°E on the equator is plotted as a function of depth and time in Fig. 5a which shows some features in common with L–R: the strength of currents at 200 m is $\sim$20 cms^{-1} in L–R, which is comparable with a typical strength of model current at that depth. At 700 m, current speeds in L–R are typically 10 cms^{-1} but on occasion are up to 17.5 cms^{-1}, compared with peak model currents of about 15 cms^{-1}. (See also Fig. 8). There thus seems to be some broad agreement as to magnitude. Furthermore, Fig. 5a shows clear upward phase propagation and a significant semi-annual signal in the 200–700 m range, again in agreement with the L–R observations.

Gent *et. al.* (1983) have modelled the response in the Western Indian Ocean and shown that the semi-annual cycle in currents originates from semi-annual forcing in the central Indian Ocean basin. (See also Fig. 3 which shows the longitudes of maximum semi-annual winds). Their model shows the existence of a focal point at a depth of 750 m at the longitude of 55°E, as proposed by Schopf, Anderson and Smith (1981). There is

also a secondary focal point near 85°E at 200 m corresponding to the 3rd vertical mode. The existence of these foci attests to the importance of the eastern boundary in creating a semi-annual cycle at depth in the Western Indian Ocean. This result is explicitly shown by Gent *et. al.* by running the model with neither boundary in which case there is no deep response, a result also shown by McCreary (1984) in his paper on wave beams, although there is no evidence for equatorial beams in the Gent *et. al.* model. Gent *et. al.* found that it is only the wind equatorward of 4° which is important in generating the response at 55°E, 0°N. There is a much larger semi-annual cycle in wind over the Arabian Sea, but it does not contribute to the equatorial response.

In Gent *et al*, only the semi-annual wind field was used to force the model whereas the full wind field is used in this study. This means that our results contain frequencies other than the semi annual. Below 200 m, the semi-annual response is dominant but certainly not a pure sinusoid. The strongest variations in currents at 600 m occur in the first half of the year as currents become first eastwards then 3 months later westwards. In the second half of the year, current variations are much weaker. Further to the east at 73°E and 90°E figs.5 b,c still show upward phase propagation although the semi-annual response is less prominent. The main band of westward currents at a fixed depth occurs later in the year the further west the observation point, consistent with westward phase propagation noted by L–R over the limited domain near 55°E which they considered.

4.3 The equatorial undercurrent

4.3.1 The Western basin

We now consider the flow in the upper 200 m. Since the best set of observations of the meridional structure of currents in the top 200 m comes from the N-S sections near 55°E taken by L-S, we will compare the model with these first. Unfortunately, however, the L-S data are only for the period mid-February to mid-June: no information is available for the latter half of the year. The L-S results show a strong eastward flow (jet) at a depth of $\sim$ 50–100 m over the whole period of their observations. Frequently, this looks

like a conventional undercurrent in that the jet lies close to, though not usually on, the equator, being more frequently found to the south of the equator than to the north. The jet can often be called a conventional undercurrent since there is westward flow above it. A conventional undercurrent then exists near the Equator from mid-February (the start of the L-S observations) to mid-April. In late April and May there is still an identifiable subsurface eastward jet but the surface flow is not westward. In late May and June there is no clear subsurface eastward jet maximum near the equator, although there is a subsurface eastward jet maximum 300 km south of the equator.

In Fig. 6 we plot the zonal current along a N-S section at 55°E for several months for comparison with the L-S observations. In March (fig.6a), a well defined, conventional undercurrent is present. Eastward flow is located slightly to the south of the equator under a strong westward flow (discussed in section 4.1), but the strength of the model undercurrent is only 40 cms^{-1} compared with observed instantaneous values of 80 cms^{-1}. Eastward flow exists to depths greater than 600 m, generally in accord with L-S observations for 1975. In April (not shown) the model undercurrent remains much as in March: it has moved to be more or less centered on the equator but its strength and depth are as in March. The main change between March and April is that the westward surface currents have retreated into the northern hemisphere and so there is not a conventional undercurrent in April although there is a subsurface eastward jet, again in agreement with L-S. By May, although the currents at 100 m have weakened only slightly there is no undercurrent as such (Fig. 6b): the surface flow is eastward and broad, extending from 5°S to beyond 10°N. This differs from L-S in that they show a distinct subsurface maximum in May in both 1975 and 1976, and a greater tendency to westward flow in the northern hemisphere. In June in the model there is a subsurface eastward jet of strength 40 cms^{-1}, located at 2–3°S. On the equator, at 80 m the flow is westward, not too unlike the structure observed in 1976, but the strength of this flow is too weak.

The L–S observations do not cover the second half of the year, but we can still analyse

the model response. There are also some Lusiad data (Taft and Knauss, 1967) in this period which will be considered later. Substantial changes in the model subsurface flow occur from June to July, associated with a southward movement of the subsurface westward flow, so that on the equator a sub-surface westward jet develops of strength 20 cms^{-1}. This increases to 40 cms^{-1} in August, beneath a westward surface flow (Fig. 6d). By October the flow south of 3°N is primarily eastward (Fig. 6e). A subsurface jet begins to form in the N.H. at ~2°N. This jet moves equatorward and by January is on the equator. Meanwhile a surface westward flow has spun-up, giving rise to a conventional undercurrent.

Returning to Fig. 5a, note that the flow at 100 m is eastward for most of the year; only in the boreal summer is it westward. In the period around January–April there is a 'conventional' undercurrent with strong westward flow at the surface and eastward flow at 100 m. Fig. 3 shows that the winds are westwards during this time. At other times when the winds are eastward, the currents at the surface and at the undercurrent depth are eastwards. There is an example of an apparent surfacing of the undercurrent in April-May following the end of the westward winds. During the late summer, there is an example at 55°E of westward flow both at the surface and at 100 m.

The results from the Lusiad expedition (Taft and Knauss,1967; see Appendix 1) are in agreement with some of these features. The location of sections in the Lusiad expedition is variable, but there is some information on flow in the Western Indian Ocean in August. In particular Fig. A section II at 53°E shows generally westward flow to considerable depth (~300 m) with eastward flow centered at ~2S° at a depth of ~100 m. Furthermore the flow is jet-like even though it is westward. Such a westward jet is also present in section III (62°E) although located somewhat deeper.

In section VII for March there is a strong undercurrent at a depth of ~80 m at 61°E, in agreement with Fig. 6a. By May (section X at 53°E) this has gone and there is generally eastward flow from the surface to ~100 m, broadly in agreement with Fig. 6b, although the eastward flow penetrates somewhat deeper in the model.

4.3.2 *The central and eastern basin*

The other longitude at which we have information on the undercurrent and upper subsurface flow for any length of time, albeit only on the equator and again only for 2 years, is at Gan 73°E. In Fig. 5b, the temporal evolution of currents at 73°E is shown for comparison with Knox's data and with the evolution further west. The response is similar to that at 55°E in that from January to March there is a 'conventional' undercurrent which appears to surface in April and to merge with the Wyrtki jet in May while in summer there is a classic reverse undercurrent, i.e. a subsurface westward jet under surface eastward flow.

In Fig. 7 we plot NS sections of zonal velocity at 73°E for (a) February, (b) May, (c) June, (d) July and (e) November. February shows a conventional U.C. but May shows westward flow at depth under a strong eastward surface flow. From February to April, the flow at 100 m is relatively persistent: it is the surface flow which changes most. From May to July a region of westward flow below the undercurrent moves upward so that by July the flow at 100 m is strongly westward. This westward flow persists through August and September. Eastward flow which starts to develop below the westward flow in September at ~150 m, develops further and rises during October and November. In January the surface flow becomes westward and we return to a more conventional undercurrent.

There are some sections from the Lusiad expedition in the eastern region which can be compared with the model though the comparison is not direct. Section VI for February (Fig. A) is located at 85°E, somewhat further east than Gan. There is westward flow to rather greater depth in Sec. VI than in the model (fig. 7a), and there is no evidence of a core of eastward flow at depth whereas there is an undercurrent in Fig. 7a. Knox (1976) has shown that the undercurrent can be a transient feature, not present each year, which could account for the difference between Sec. VI and Fig. 7. In Sec. IX, there is a very marked undercurrent at 92°E in April. In the model (Fig. 5c) there is strong eastward flow at depth consistant with the Lusiad data but the surface flow is eastward contrary to sec IX. In September (Sec. IV) there is a strong reverse undercurrent at 79°E also exhibited

in the model (see Fig. 5b). The deep (below 200 m) westward flow in the NH in Sec V in September is not obvious at 73°E (not shown), although a reasonably deep westward flow is present in October.

At 90°E (Fig. 5c) there is a classic undercurrent in the sense of having surface westward flow above an eastward jet only very briefly in February/early March, but since the subsurface flow is much more strongly eastward than the surface flow from early January to late March, one could consider there to be an undercurrent at 90°E from January to March. Fig. A panel VI shows no such undercurrent however. Another interesting feature of Fig. 5 is that while there is a significant semi-annual variation in the surface flow, this is much less pronounced at undercurrent depths.

From the time sequences at discrete points given in Fig. 5 and also from the latitudinal cross-section in fig. 6 and 7, it is difficult to see the spatial coherence of the flows, so in Fig. 8 the zonal currents along the equator are plotted at bimonthly intervals. Eastward flow at ~100 m is very marked all along the equator in February, March and April while westward flow dominates from June to September. In November and December the flow is mainly eastward though not quite like an undercurrent.

4.4 Wave propagation

In the previous sections wave beams, or even wave foci, were not obvious in the results presented. Nonetheless there are certain depths where a wave interpretation is useful. In Fig. 9 the velocity at 666 m (model level 12) is shown for May, July and September; there is nothing special about this selection of months other than that it shows westward propagation and gives another slant on the semi-annual signal observed in Fig. 5a in the west. This westward propagation appears to be Rossby wave like and this can be partly confirmed by Figs. 10a and 10b which show the zonal velocity at 666 m on the equator and at 5°S. The speed of propagation at 5°S is 60° in 6 months while at 10°S it is 14° in 6 months (not shown). The ratio of speeds is approximately a factor of 4 between 5°S and 10°S, more or less what one would expect from a Rossby wave with eastward velocity given

by $\beta c^2/f^2$. The speed of propagation of this largely semi-annual wave at 10°S corresponds to a value for c of 1.3 ms^{-1}, rather close to a 2nd mode speed. On the equator the speed of propagation is faster; no unique speed seems clearly identifiable but signals seem to propagate somewhere around 50 cms^{-1}. For a second mode, the fastest equatorial Rossby wave would travel at $\sim c/3$ giving a value for c of $\sim$ 1.5 ms^{-1}, consistent with the value obtained at 10°S.

There are no extensive data records at this depth in the Indian Ocean to confirm the model response but the signal does seem to stand out clearly, and hopefully observations will be sought at some stage to confirm its existence. Note that Fig. 10a shows that at 55°E a typical amplitude of the semi-annual signal at 666 m is 14 cms^{-1}, comparable to the strength of the observed current variation of L-R. The amplitude is greatest in the central equatorial region but weak near the eastern boundary.

4.5 Dynamic Topography

The temporal variation in the surface dynamic height relative to 800 m has been calculated but is not shown. In February there is almost no dynamic height gradient in the zonal direction in the near equatorial region. The zonal gradient is still weak over a substantial part of the equatorial region in March (differences between east and west of ~5 dyn cms). The dynamic height begins to increase in the east in April. From then through the summer the gradient increases as dynamic height rises in the east before starting to fall in November. There have been a number of measurements of dynamic height. During the Lusiad expedition, an E-W difference of approximately 18 dyn cms was measured in July, and less than 4 dyn cms in March. The latter value is not at variance with the model results which in March show an E-W difference of ~5 dyn cms. In July, however, there is a substantial gradient along the equator with the east some 25 dyn cms higher than the west, bigger than the Lusiad results (and in June the E-W difference is slightly stronger still). Eriksen (1979) found a difference in dynamic height between the eastern and western equator of 33 dyn cms in December which is larger than the model

value of approximately 25 dyn cms.

The dynamic height at 113 m relative to 798 m is shown, together with the zonal flow at 113 m, in Fig. 11a, b. This level was chosen as representative of the undercurrent. From September to March, dynamic height stands higher in the west than in the east. This gradient is favourable for undercurrent development. Eastward flow continues to increase during this period reaching a maximum in March. By April the pressure gradient is small (even though there is a gradient at the surface in the eastern ocean) and the eastward flow starts to weaken. In May to June the pressure gradient is adverse to an undercurrent and the eastward flow continues to weaken. The pressure gradient is nearly back to zero by July except in the west. Around August a minimum in dynamic topography develops near 80°E. Although the pressure gradient to the east of this is in a direction to drive westward flow, the westward flow does not in fact increase but decreases although east than further west. Figs. 11a and 11b show that there is not a close correspondence in detail between undercurrent strength and pressure gradient but that there are substantial lags between the currents and the pressure gradient.

5. Discussion

The model results raise some interesting questions about the nature of equatorial undercurrents. Classical models of the undercurrent have been developed, most recently by Pedlosky (1988). Elegant theoretical interpretations of the undercurrent and its temporal changes are given by Cane (1980) and Philander and Pacanowski (1980). However, Cane's model is considerably simpler than the real ocean: nonlinear processes are probably exaggerated, the model is only half as wide as the Indian Ocean and in order to isolate physical processes a simplified wind forcing is used. The Philander and Pacanowski model is more comprehensive but the wind fields in that study too are over simplified. Fig. 3 shows that the wind field over the Indian ocean, both spatially and temporally, is much more complicated than that used in the idealised calculations. Nonetheless some of the results are sufficiently appealing that they may apply despite these limitations.

For example, in the idealized case the initial subsurface response to eastward winds is rapid and local, whereas the response to westward winds is slow. This is not obviously borne out by the model results given in this paper, however. The actual winds change from being westward to eastward in March–April (earlier in the east), and although there is a rapid change in the surface flow, there is little sign of any significant change in the flow at undercurrent depth (see Fig. 8). The flow is already eastward in February, partly as a response to westward winds, and this is broadly maintained through May. (There are some regional adjustments. For example the position of strongest eastward flow is in the far east in February whereas it is further west in April.) The typical strength of the eastward flow at $\sim$40 cms^{-1} is not much altered, despite the fact that the winds have become considerably more eastward over this time.

One reason for the large discrepancy between these results and those obtained using simpler wind fields is that the actual wind field over the Indian ocean differs from the idealised winds to such a large degree. When the real wind changes in the early part of the year from being westward to eastward, the undercurrent response is a combination of the response to a decaying westward wind stress (which is slow according to Cane and Pacanowski and Philander) and the response to an increasing eastward wind stress (which is fast). It is therefore difficult to use these ideas in interpreting actual undercurrent features.

The occurrence of westward flow at undercurrent depth in June–September is interesting. In Cane's model, westward flow is only produced by turning on a cross equatorial wind as westerlies are turned off, which induces a meridional movement of the undercurrent bringing westward flow to the equator. It is unlikely that the westward flow in the model described here results for this reason. Fig. 7b for May shows that at Gan the flow off the equator is eastward in both hemispheres and therefore cannot be the source of the westward currents. The specific occasion to which Cane applied the upwind movement of the undercurrent was January 1974 but since our model reproduces only an average

seasonal cycle we cannot comment on specific years. Further west, at 55°E, L-S noted a movement into the southern hemisphere of the undercurrent and Fig. 6 is not inconsistent with the subsurface eastward flow moving upwind.

The time of occurrence of subsurface westward flow is not easily related to a relaxation of eastward winds either. An eastward surface flow should decay rapidly when the source of eastward momentum is switched off. The pressure gradient is westward and, until waves arrive to alter it, should act to retard the eastward surface flow and reverse it. Likewise, the subsurface eastward flow should weaken and if the pressure gradient has long enough to act it too should become westward. Eastward winds do start to weaken in June in the western half of the basin, but not in the east where the subsurface currents first become westward. The changes therefore appear to be a result of non-local transients transmitted by waves rather than a result of local processes.

The presence of westward flow at undercurrent depth has been noted by Knox (1976) and L-S, at the same times of the year as in the model. There seems to be more vertical sheer in the model than in Knox's observations, however, indicating that in the model westward undercurrent flow can lie beneath strong eastward flow near the surface. Examples of strong shear can be found in the Lusiad data (see Appendix 1).

Following the weakening of westward winds in February, there are examples of the surface flow rapidly becoming eastward, giving the impression of a surfacing of the undercurrent (see Fig. 5) as suggested by Philander and Pacanowski (1980).

Analysis of the direction of the equatorial current structure of the upper 200 m and of the lateral and temporal movements in this region, give a different perspective on what is meant by an undercurrent. There are occasions in January, February and March when a classical undercurrent is present over most of the Indian ocean, i.e. there is eastward flow at undercurrent depth beneath surface westward flow, but there are cases when there is strong eastward flow beneath weaker or stronger surface eastward flow. Is this an undercurrent? And there are reverse undercurrents, when the flow at ~100 m is westward beneath a

surface eastward flow.

Lateral movements of the undercurrent core are not confined to ~1° of the equator. The eastward flow may migrate to the south several degrees to become part of the south equatorial countercurrent. At what latitudes does the flow cease to be called an undercurrent. Clearly the classical ideas of undercurrents, or the more recent, but steady connections to mid latitudes, are much more complicated than suggested by Pedlosky (1988).

6. Summary

A GCM of the Indian ocean has been run, forced by Hellerman and Rosenstein wind stress. The equatorial currents from this model have been compared with ship drift observations, as well as the time series at 73°E (Gan) and at 55°E. The model is capable of simulating the temporal evolution of surface currents quite well, both in amplitude and phase though there might be a slight tendency to over-predict the strength of the Wyrtki jet in May. The model also simulates a classical undercurrent in February–March which compares favourably with observations at 55°E and 73°E (though it obviously cannot simulate the inter-annual variability such as observed at both these sites). The model undercurrent is a basin-wide feature in February/March.

The theoretical studies of Cane 1980 indicate that the flow in response to both easterly and westerly wind stress is eastward at undercurrent depth: in his model westward flow at undercurrent depth only results from the action of a cross-equatorial wind moving the current field upwind leading to a replacement of eastward flow at the equator by westward flow previously off the equator. The model response described in this paper seems to be at variance with this in some respects, as it is not difficult to produce westward flow at 100 m and indeed westward flow exists for several months in the summer time. In the east, it does not seem to be an obvious result of upwind displacement of the current pattern, although this may be partly so at 55°E. The undercurrent response at Gan (73°E) seems to be too complicated to be interpreted in simple terms, involving vertical movements of currents as

well as meridional movements. Waves associated with vertical modes are undoubtedly an important component of the response of the undercurrent to the surface wind changes, but it is in general not easy to identify them. The amplitude of the undercurrent in general appears to be too weak.

In the region below 200m, the model shows a semi-annual cycle; this has upward phase propagation, consistent with Leetmaa and Stommel (1980), but has a weaker amplitude than that observed by L-R in the 200–600m band. There is also an east to west phase motion. Although it is not in general easy to separate the non local wave response from local processes, at 666 m, there is a clear east to west motion which is very suggestive of a long Rossby wave. The stacked vertical jets observed by Luyten and Swallow (1976) and by Ponte and Luyten (1990) are not well modelled below 600 m.

References

Anderson, David L.T. (1976) The low-level jet as a western boundary current. *Mon. Weather Rev.* 104, *907-921.*

Anderson, David L.T., D. Carrington, R.A. Corry and C. Gordon (1991) Modelling the Somali Current. *J. Mar. Res.*

Anderson, David L.T.A., and D.J. Carrington (1992) Modelling interannual variability in the Indian Ocean using momentum fluxes from the UKMO and ECMWF operational weather analyses. In preparation.

Cadet, D. and B. Diehl (1984) Interannual variability of surface fields over the Indian Ocean during recent decades. *Monthly Weather Review* 112, October 1984.

Cane, M. (1980) On the dynamics of equatorial currents, with applications to the Indian Ocean. *Deep-Sea Res.*, 27A, *525-4.*

Carrington, D.J. (1990) An Ocean General Circulation Model of the Indian Ocean for hindcasting studies. U.K. Met. Office Climate Research Technical Note No. 2 (October 1990).

Cox, M. (1984) A primitive equation, 3-dimensional model of the ocean. *GFD2 Ocean Group, Technical Report No. 1 Princeton N.J..*

Cresswell, G.R., M. Fieux and J. Gonella (1981) The Wyrtki equatorial jet, May/June 1980. *Tropical Ocean-Atmosphere Newsletter*, 5, (unpublished manuscript).

Cutler, A. and J. Swallow (1984) Surface currents of the Indian Ocean (to 25°S, 100°E): compiled from historical data archived by the Meteorological Office, Bracknell, UK. *Institute of Oceanographic Sciences, Report, No. 187 8pp. and 36 charts.*

Eriksen, C.C. (1979) An Equatorial Transect of the Indian Ocean. *Journal of Marine Research*, 37, *215-232.*

Esbensen, S.K. and Y. Kushnir (1981) The heat budget of the global ocean: an atlas based on estimates from marine observations. *Report No. 29 Climate Research Ins. Oregon State University, Corvallis.*

Gent, P.R., and J.R. Luyten (1985) How much energy propagates vertically in the equatorial oceans? *J. Phys. Oceanogr.*, 15, *997-1007.*

Gent, P., K. O'Neill and M. Cane (1983) A model of the semi-annual oscillation in the equatorial Indian Ocean. *J. Phys. Oceanogr.*, 13, *2148-2160.*

Gill, A.E. (1980) Some simple solutions for heat-induced tropical circulation. *Q.J.R. Meteorol. Soc.* 106, *447-462.*

Han and Lee (1983) An analysis of monthly mean wind stress over the global ocean. *Monthly Weather Review*, **111**, *1554-1566.*

Hellerman, S. and M. Rosenstein (1983) Normal monthly wind stress over the world ocean with error estimates. *J. Phys. Oceanogr.*, 13, *1093-1104.*

Jerlov, N.G. (1968) Optical Oceanography. *Elsevier, 194 pp.*

Kawase, M. (1987) Establishment of deep ocean circulation driven by deep-water production. *J. Phys. Oceanogr.*, 17, *2294-2317.*

Knox, R. (1976) On a long series of measurements of Indian Ocean equatorial currents near Addu Atoll. *Deep-Sea Res.*, 23, *211-221.*

Knox, R.A. and M.J. McPhaden (1980) Profiles of velocity and temperature near the Indian Ocean Equator. Scripps Inst. of Ocean. Ref No. 80-6.

Leetmaa, A. and H. Stommel (1980) Equatorial current observations in the western Indian Ocean in 1975 and 1976. *J. Phys. Oceanogr.*, 10, *258-269.*

Legler, D.M., I.M. Navon and J.J. O'Brien (1989) Objective analysis of pseudo-stress over the Indian Ocean using a direct-minimization approach. *Mon. Wea. Rev.*, 117, *709-720.*

Luyten, J.R., M. Fieux and J. Gonella (1980) Equatorial currents in the western Indian Ocean. *Science*, 209, *600-603.*

Luyten, J. and D. Roemmich (1982) Equatorial currents at semi-annual period in the Indian Ocean. *J. Phys. Oceanogr.*, 12, *406-413.*

Luyten, J. and J. Swallow (1976) Equatorial undercurrents. *Deep-Sea Res.*, 23, *1005-1007.*

Matsuno, T. (1964) Quasi-geostrophic motions in equatorial areas. *J. Meteorol. Soc. Japan* 2, *25-43.*

McCreary, J. (1981) A linear stratified ocean model of the equatorial Undercurrent. *Phil. Trans. Roy. Soc. London A.* 278, *603-635.*

McCreary, J. (1984) Equatorial beams. *J. Mar. Res.*, 42, *395-430.*

McPhaden, M.J. (1984) On the dynamics of equatorial subsurface countercurrents. *J. Phys. Oceanogr.*, 14, *1216-1225.*

McPhaden, M.J., J.A. Proehl and L.M. Rothstein (1986) The interaction of equatorial Kelvin waves with realistically sheared zonal currents. *J. Phys. Oceanogr.*, 16, *1499-1515.*

Pacanowski, R. and S.G.H. Philander (1981) Parameterization of vertical mixing in numerical models of tropical oceans. *J. Phys. Oceanogr.*, 11, *1443-1451.*

Paulson, C.A., and J.J. Simpson (1977) Irradiance measurements in the upper ocean. *J. Phys. Oceanogr.*, **7**, *952-956.*

Pedlosky, J. (1987) An inertial theory of the equatorial undercurrent. *J. Phys. Ocean.* 17, *1978-1985.*

Philander, S.G.H. and R.C. Pacanowski (1980) The generation of equatorial currents. *J. Geophys. Res.*, 85, *1123-1136.*

Ponte, R.M. and J. Luyten (1990) Deep velocity measurements in the western equatorial Indian Ocean. *J. Phys. Oceanogr.*, 20, *44-52.*

Reverdin, G. (1987) The upper equatorial Indian Ocean. The climatological seasonal cycle. *J. Phys. Oceanogr.*, **17**, *903-927.*

Rothstein, L.M., D.W. Moore and J.P. McCreary (1985) Interior reflections of a periodically forced equatorial Kelvin wave. *J. Phys. Oceanogr.*, 15, *985-996.*

Rothstein, L.M., M.J. McPhaden and J.A. Proehl (1988) Wind-forced wave-mean flow interactions in the equatorial waveguide: I. The Kelvin wave. *J. Phys. Oceanogr.*, 18, *1435-1447.*

Schopf, P., D.L.T. Anderson and R. Smith (1981) Beta-dispersion of low-frequency Rossby waves. *Dyn. Atmos. Oceans*, 5, *187-214.*

Swallow, J.C. (1964) Equatorial undercurrent in the Indian Ocean. *Nature*, 204, *436-437.*

Swallow, J.C. (1967) The equatorial undercurrent in the western Indian Ocean in 1964. *Studies in Tropical Oceanography*, 5, *15-36*, University of Miami Press, Coral Gables, Fla.

Taft, B. and J. Knauss (1967) The Equatorial Undercurrent of the Indian Ocean as observed

by the Lusiad Expedition. *Bull. Scripps Inst. Oceanogr.*, 9.

Wyrtki, K. (1973) An equatorial jet in the Indian Ocean. *Science*, 181, *262–264.*

Wunsch, C. (1977) Response of an equatorial ocean to a periodic monsoon. *J. Phys. Oceanogr.*, 7, *497–511.*

Yoshida, K. (1959) A Theory of the Cromwell current and of the equatorial upwelling, *Journal of the Oceanographical Society of Japan*, 15, *154–170.*

Table 1

AUTHOR	LOCATION	DATE	COMMENTS
Taft and Knauss 1967	Various	1962-63	See App 1 for some N-S sections of velocity) (The Lusiad expedition).
Swallow (1964, 1967)	58°E	March 1964 June 1964	
Duing *et al.* (1967)	58°E	Jan 1965	
Bruce (1973)	55°E 51°E	Aug, Sept 1964 1970	
Luyten & Swallow (1976)	53°E	16 May – 17 June 76	Top to bottom profiler data
Luyten & Roemmich (1982)	47°E–59°E	May 79 to May 80	Current meter data between 200 m and 700 m
Leetmaa & Stommel (1980)	55°E	Feb-June 75 Feb-June 76	Upper 250 m
Ponte & Luyten (1990)	47°E-62°E	Apr-June 1979	Top to bottom profiler data
Knox (1976)	73°E	Sept 72-Apr 75	Upper 100 m

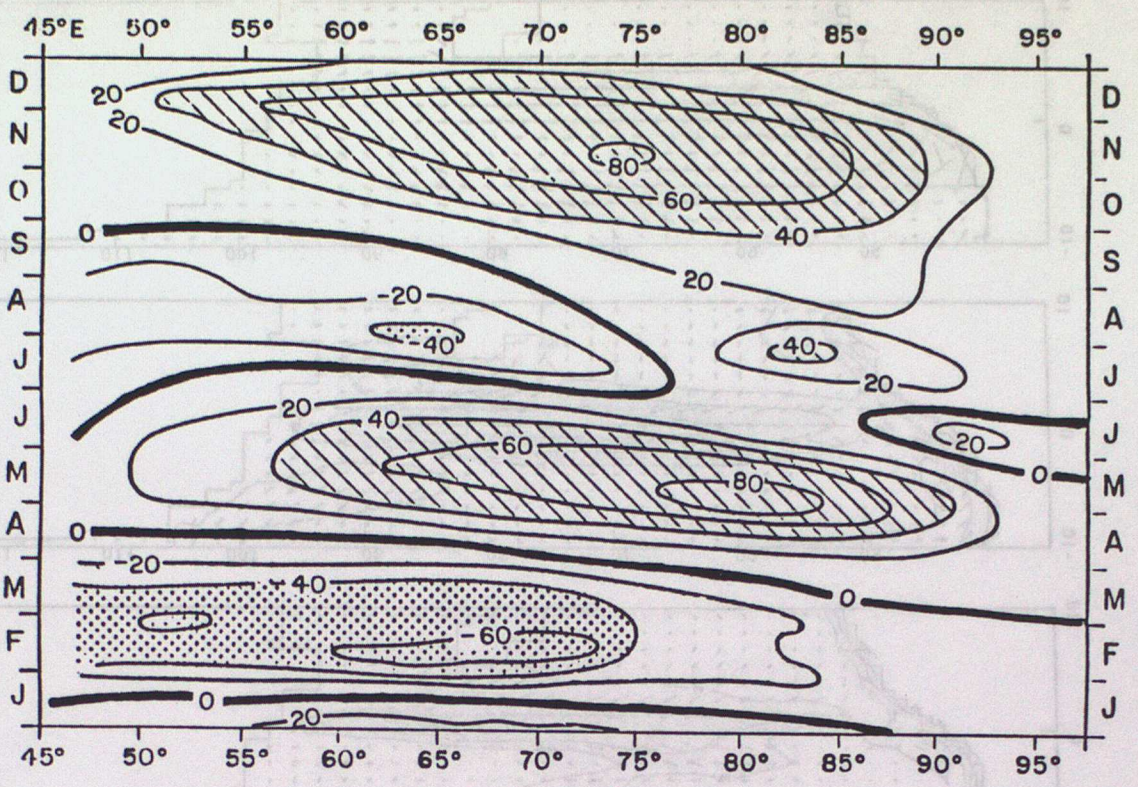

Fig. 1a: The temporal evolution of zonal surface currents along the equator in the Indian ocean, based on the Swallow and Cutler atlas of ship drift currents. This figure shows not only the strong eastward currents in May and November (the Wyrtki jet), but also strong westward flow in February and moderately strong westward flow in July–September in the western half of the basin. From Reverdin (1987). (Positive values: eastward currents. Shading: $>40 cms^{-1}$; stippling: $< -40 cms^{-1}$).

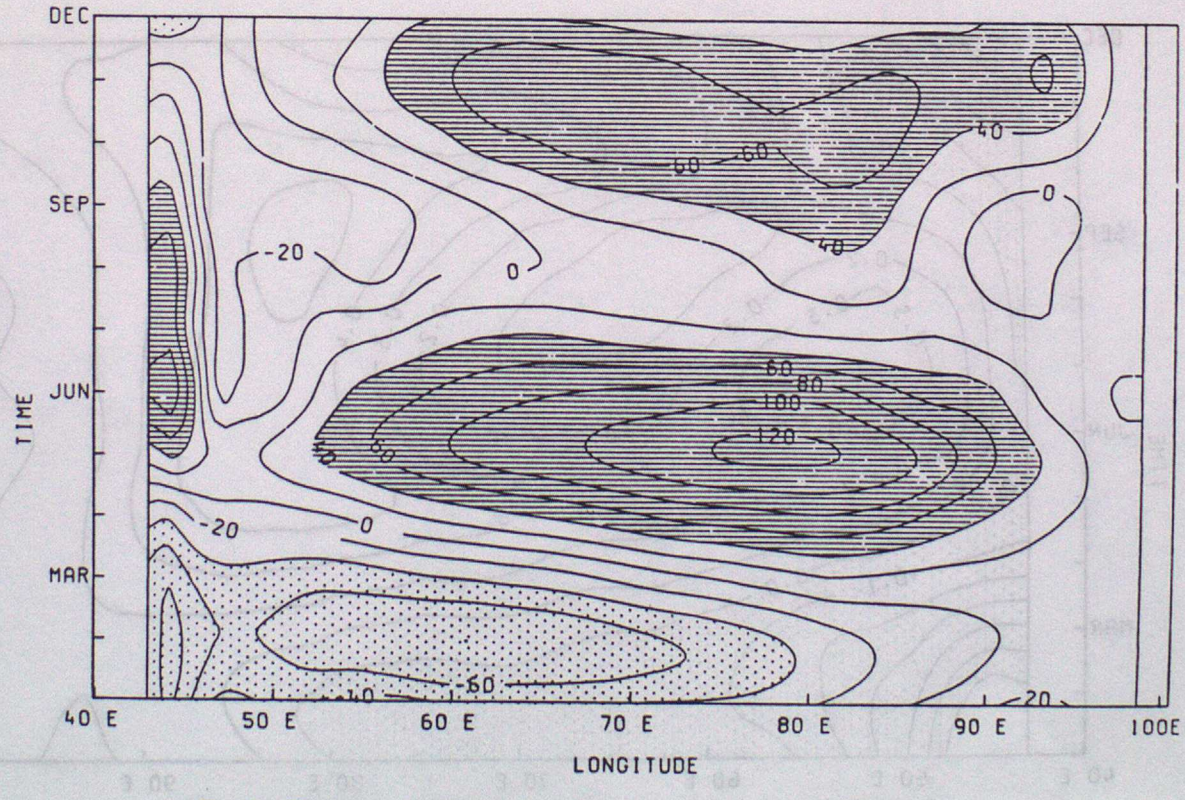

Fig. 1b: The temporal evolution of zonal surface currents along the equator from the Indian ocean model for comparison with Fig. 1a (shading and stippling as in Fig. 1a). Broad features are similar, in particular the occurrence of the Wyrtki jet in May and November. Current strengths are a little different to Fig. 1a with the modelled Wyrtki jet much stronger in May than in November compared to the observed strengths which are about equal.

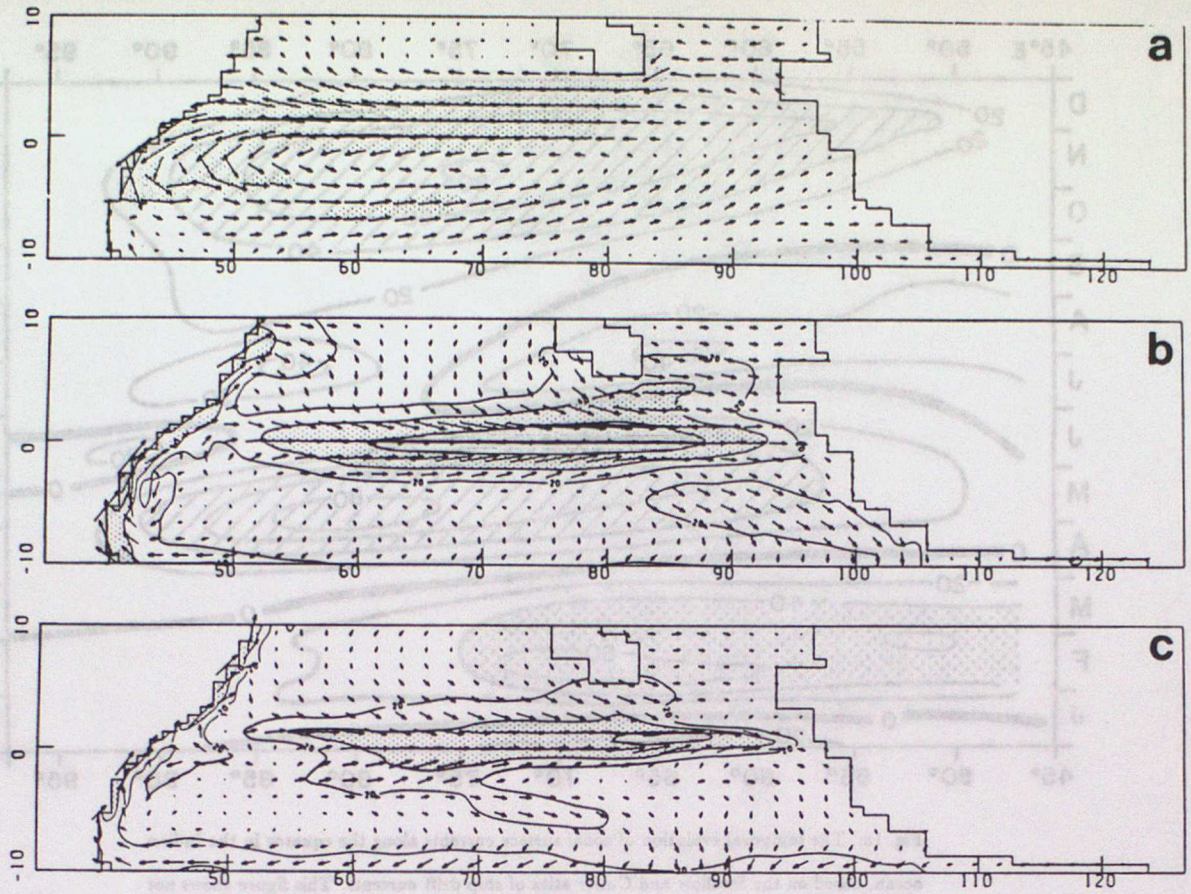

Fig. 2: Model surface current in (a) February, (b) May and (c) October, showing the strong eastward jet at the pre and post monsoon periods (May and October). In February there is a strong westward flow in excess of 1 ms^{-1}. The eastward flow of the Wyrtki jet is much narrower than the westward flow. (Light shading: 40–60 cms^{-1}; heavier shading: >60 cms^{-1}).

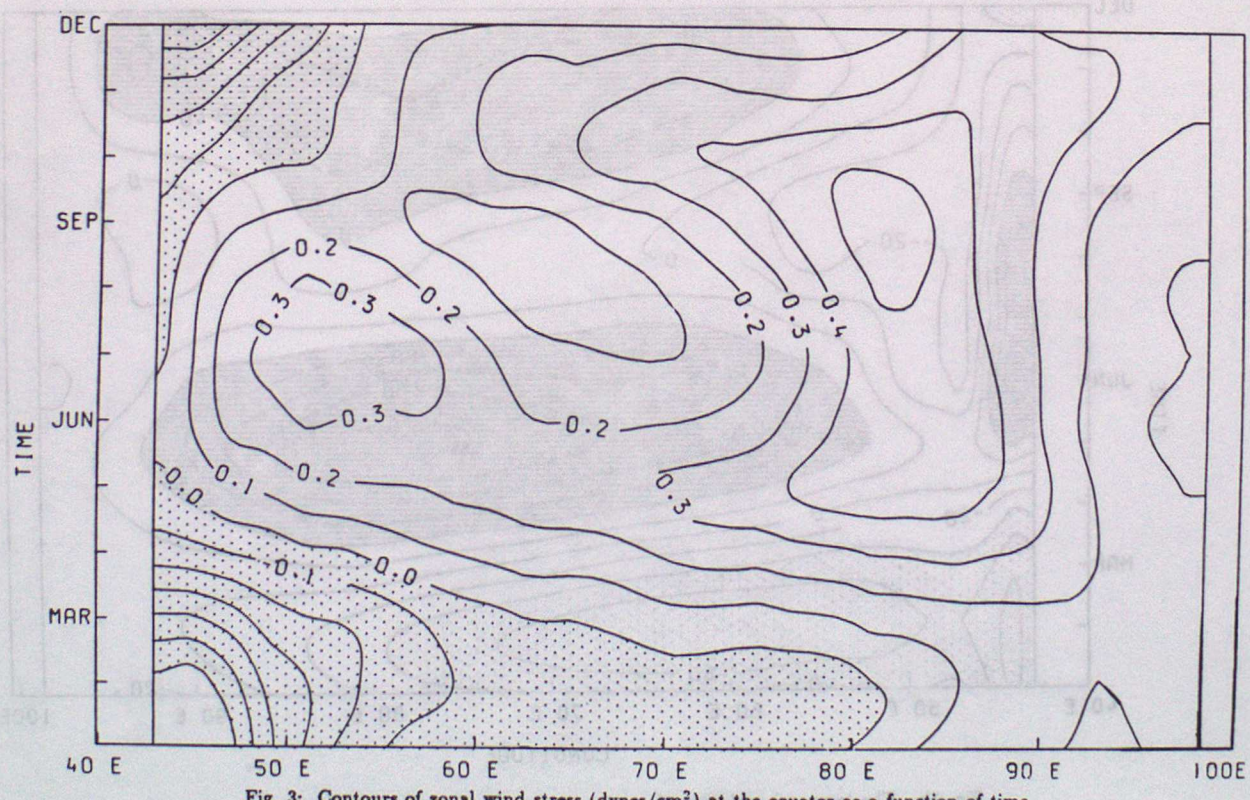

Fig. 3: Contours of zonal wind stress (dynes/cm^2) at the equator as a function of time (westward stress shaded). Westward winds are present in the western half of the basin in the early part of the year, but the winds over the Indian ocean are mainly eastward. During the S.W. monsoon, eastward winds increase in the western and eastern parts of the basin, but decrease in the centre of the basin. Such strong spatial and temporal variation excites many wave modes in the ocean.

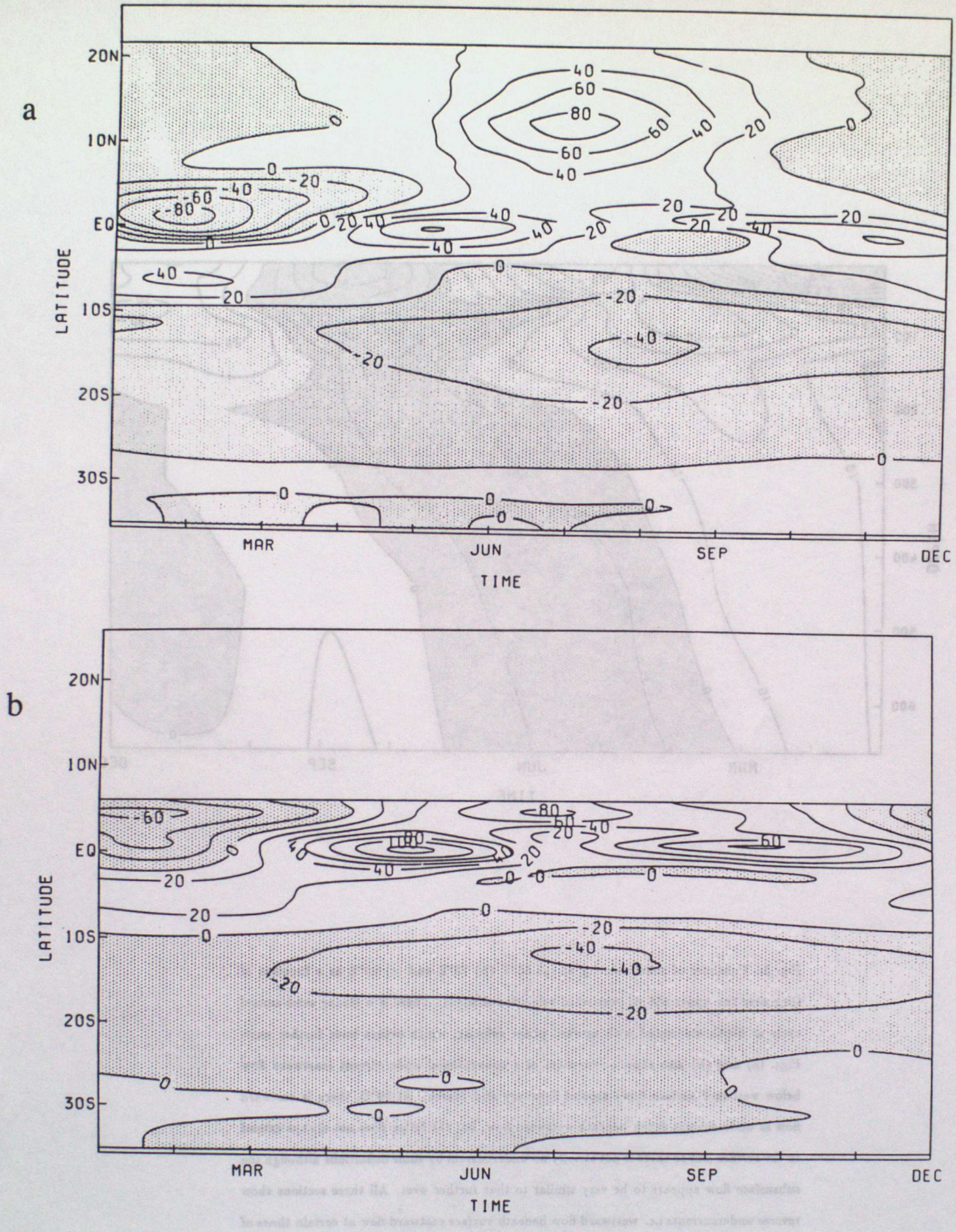

Fig. 4: Temporal variations in surface zonal flow (westward velocities shaded) along North-South sections at (a) 60°E and (b) 80°E, showing that the near equatorial westward flow in January to April is strongest in the west and to the north of the equator. The eastward Wyrtki jet is stronger at 80°E, where the equatorial flow is eastward all year, except in January to March. The strong westward flow at 60°E can result from a relaxation of eastward winds inducing a surge as well as from a local response to westward winds.

a

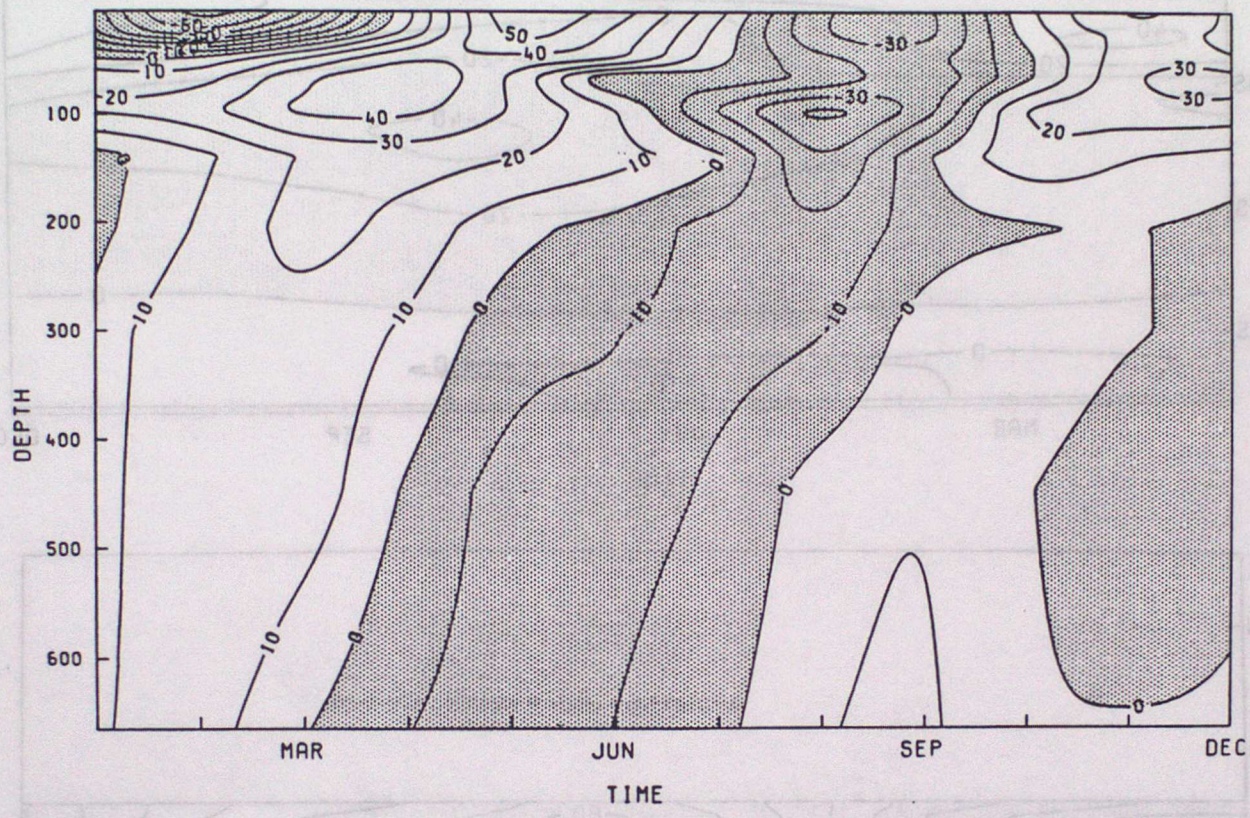

Fig. 5: Contours of zonal velocity at (a) 55°E (b) 73°E and (c) 90°E as a function of time over the upper 666 m (westward velocities shaded). There is a strong semi-annual cycle at depth associated with upward phase velocity, which occurs later further west. Figs. (a) and (b) also show occurrences of a conventional undercurrent (eastward flow below westward surface flow) around February and March. At 90°E, there is eastward flow at undercurrent depth beneath westward flow, but the latter does not always extend to the surface and so there is not strictly an undercurrent by some definitions although the subsurface flow appears to be very similar to that further west. All three sections show reverse undercurrents i.e. westward flow beneath surface eastward flow at certain times of year.

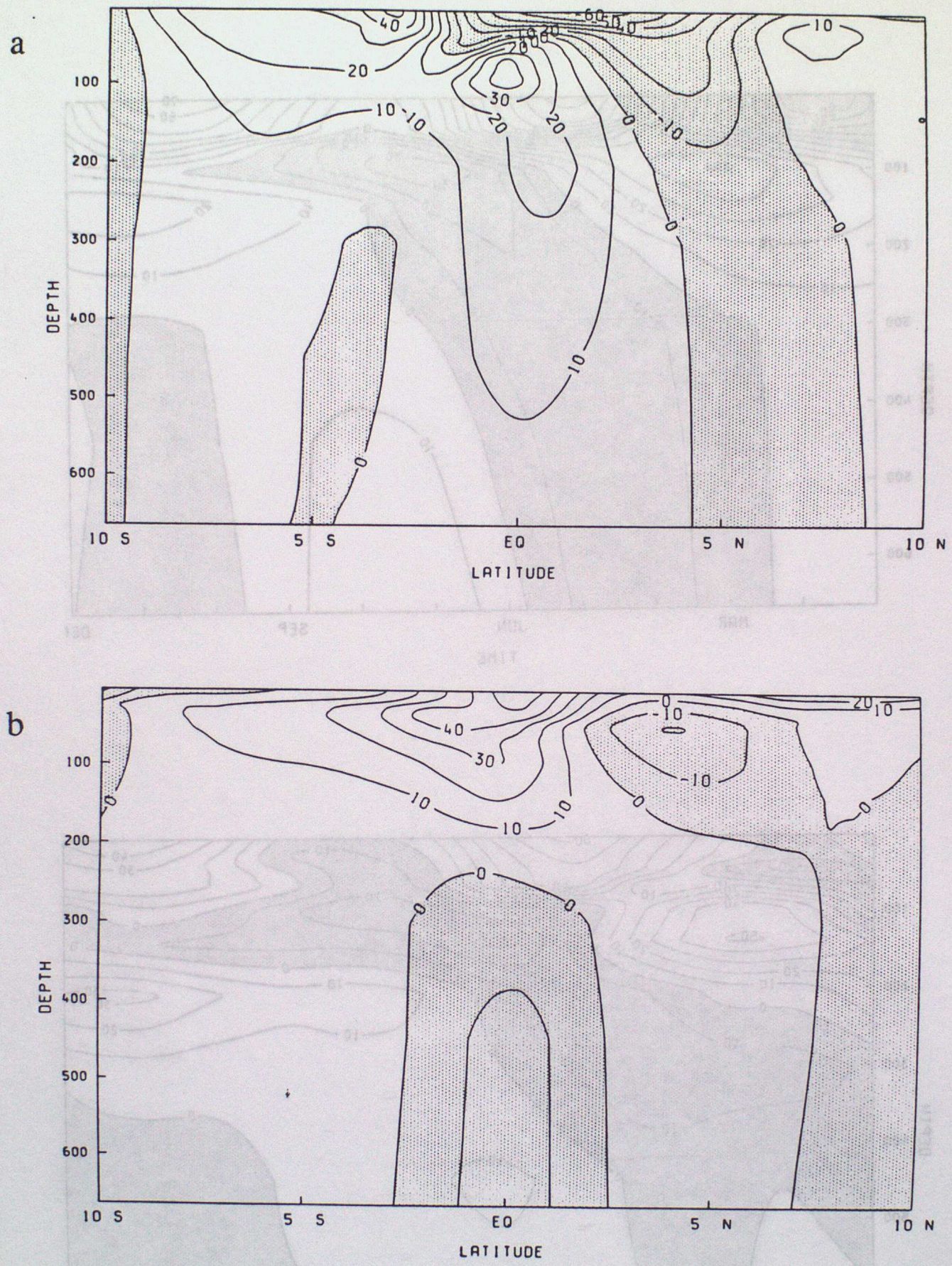

Fig. 6: N-S sections of zonal flow at 55°E for (a) March, (b) May, (c) June, (d) August and (e) October. (Westward velocities shaded.)

b

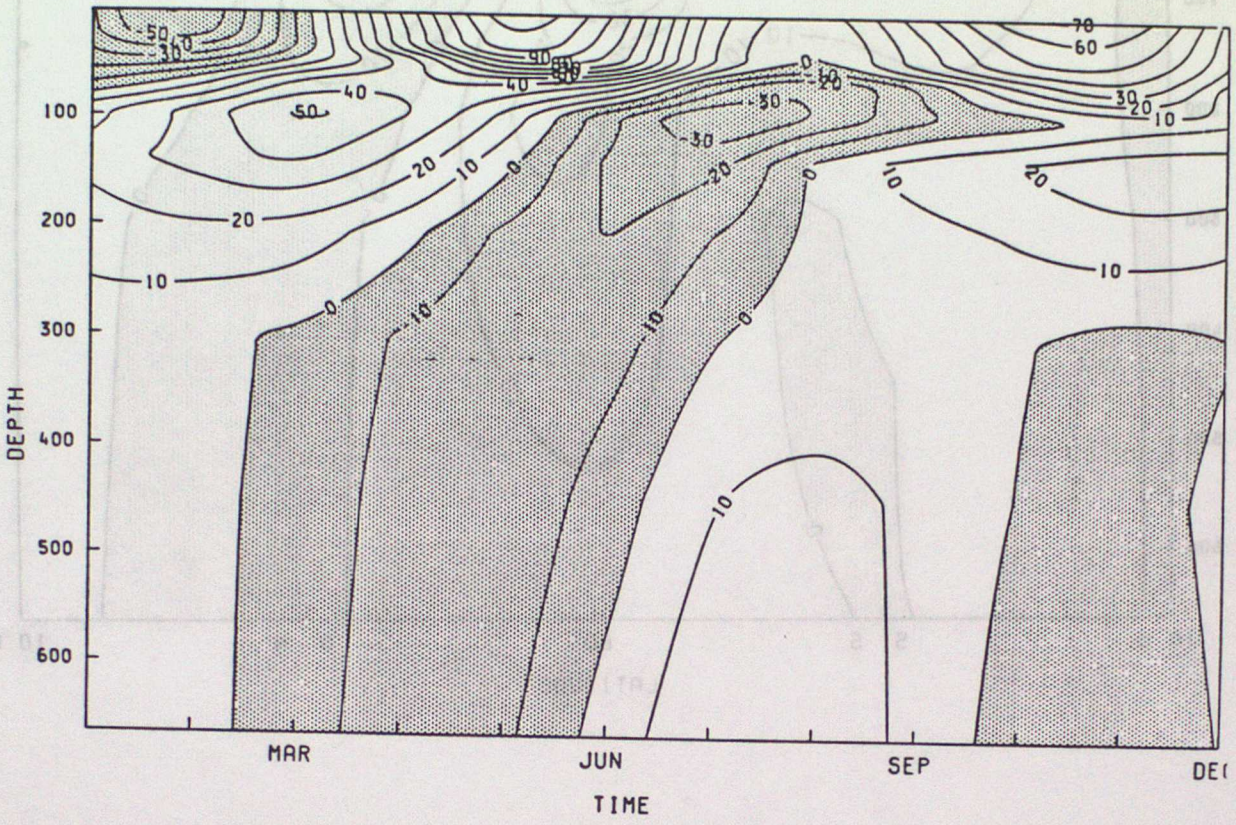
DEPTH
100
200
300
400
500
600
MAR
JUN
SEP
DEC
TIME

c

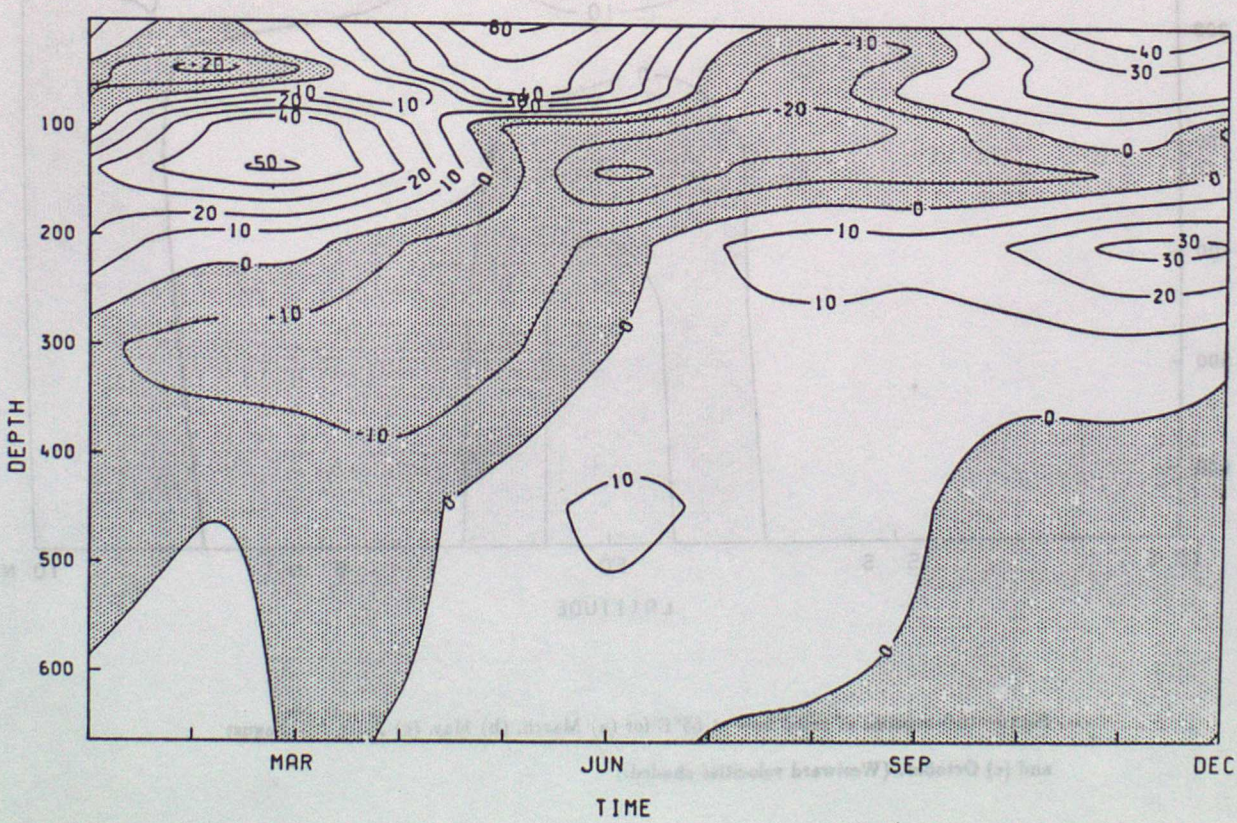
DEPTH
100
200
300
400
500
600
MAR
JUN
SEP
DEC
TIME

c

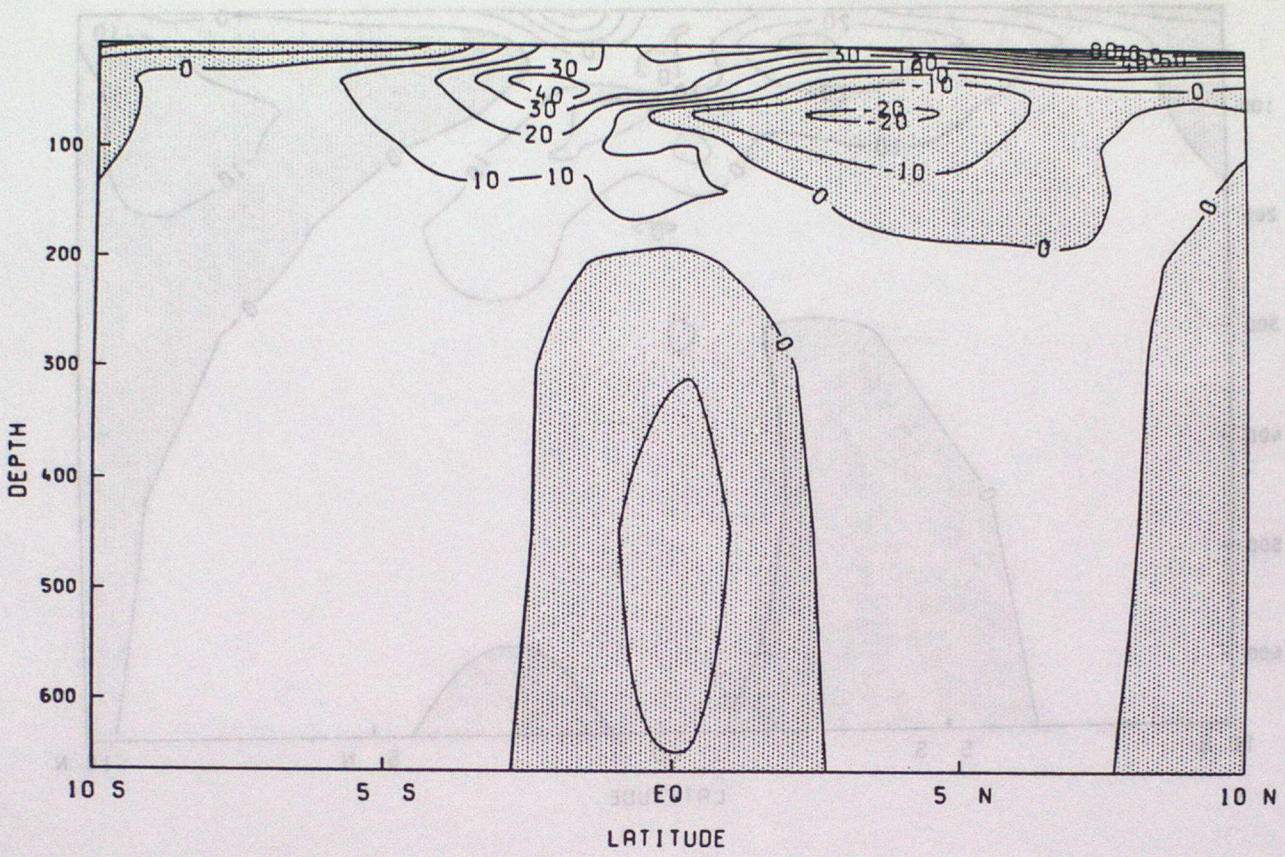
DEPTH
100
200
300
400
500
600
10 S
5 S
EQ
5 N
10 N
LATITUDE

d

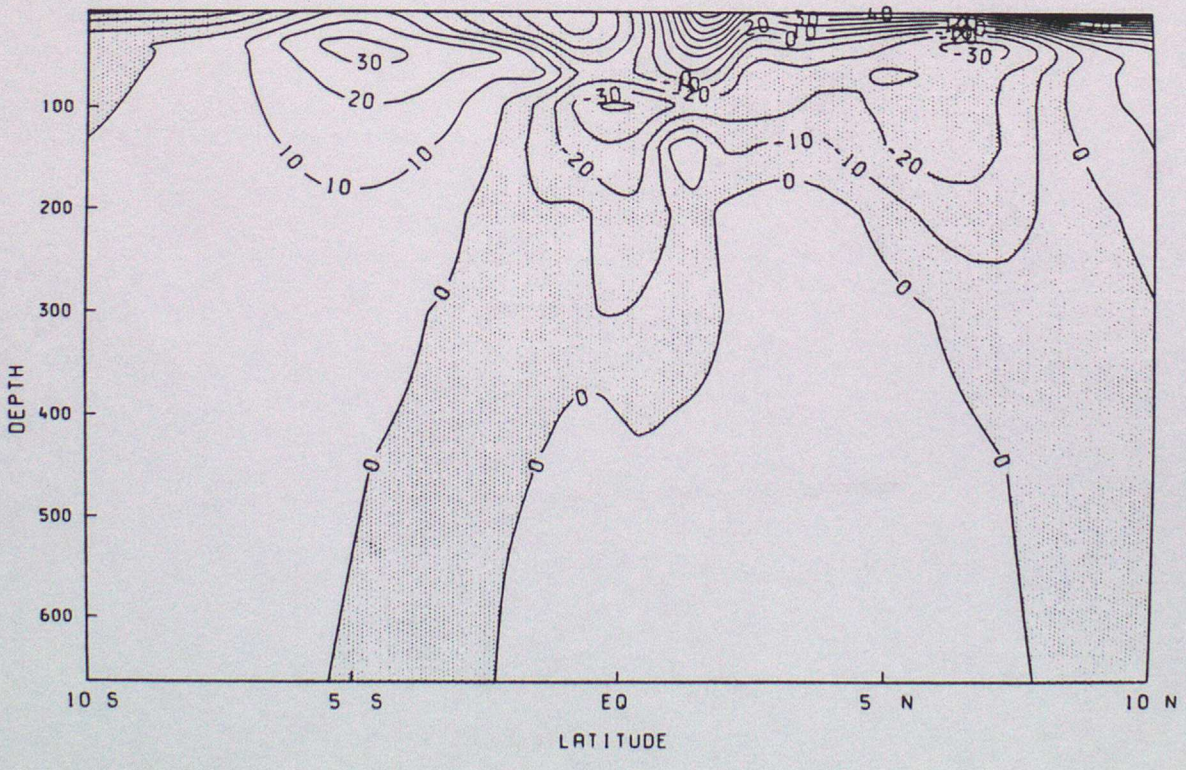
DEPTH
100
200
300
400
500
600
10 S
5 S
EQ
5 N
10 N
LATITUDE

e

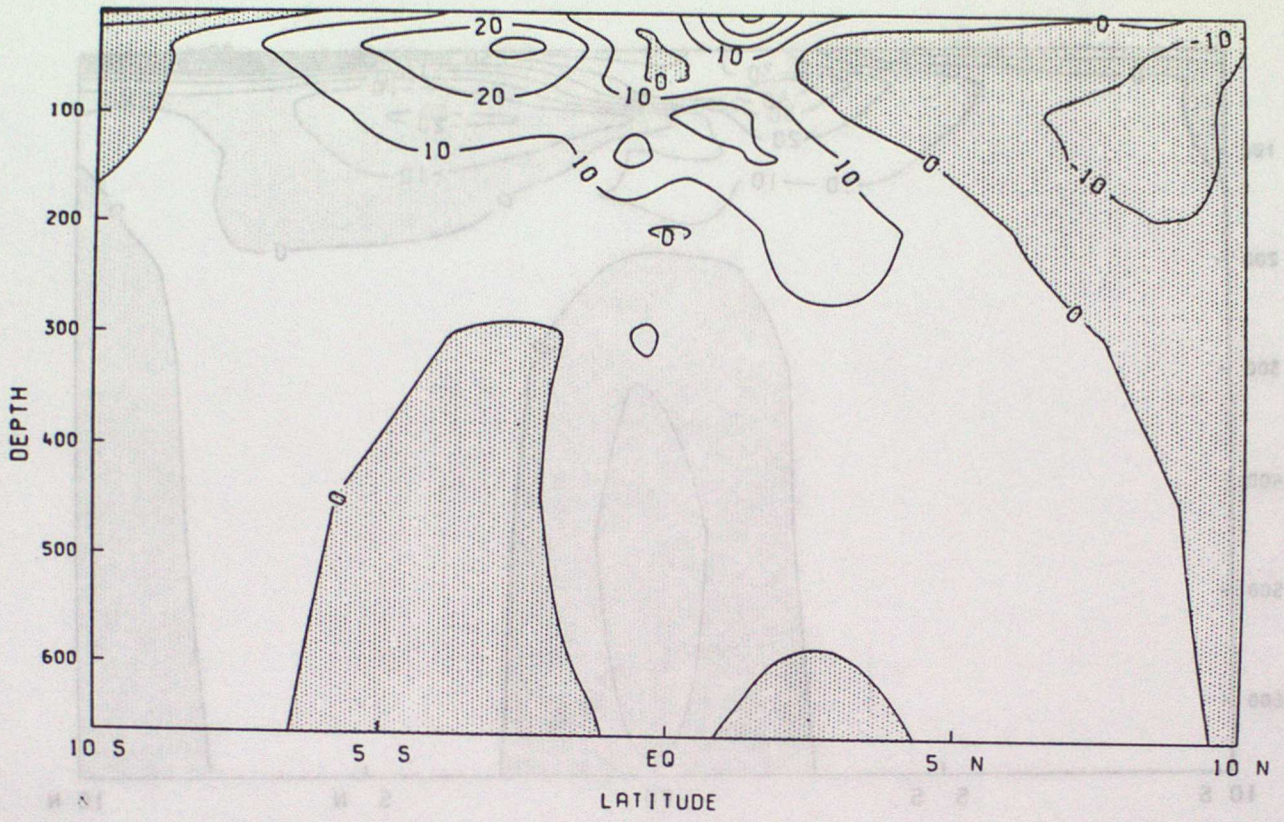

DEPTH
100
200
300
400
500
600
10 S
5 S
EQ
5 N
10 N
LATITUDE
20
20
10
10
10
10
10
0
0
0
0
0
-10
-10

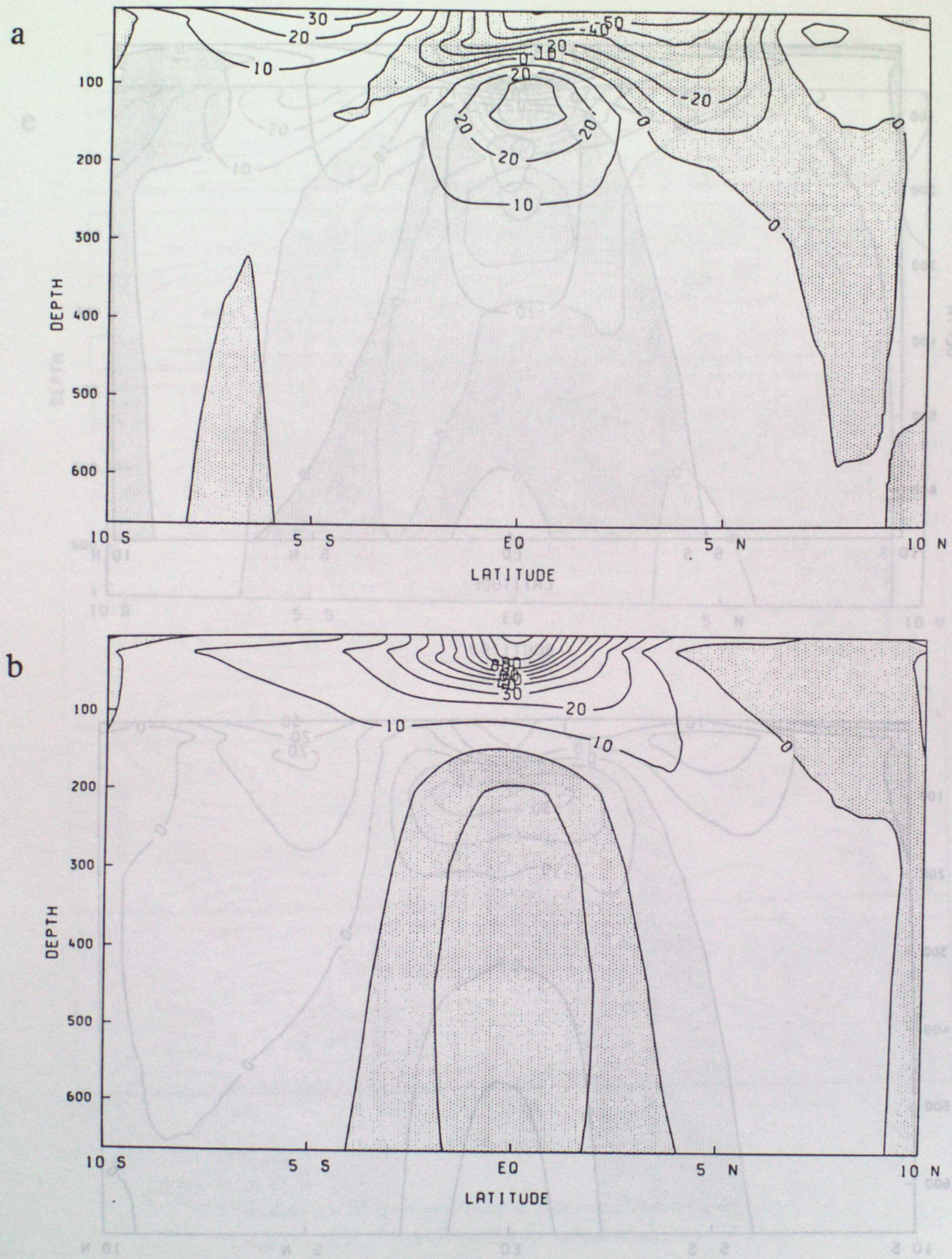

Fig. 7: N–S sections of zonal flow at 73°E (Gan) for (a) February, (b) May, (c) June, (d) July and (e) November. A classical undercurrent is present in February, and a reverse undercurrent in July. (Westward velocities shaded).

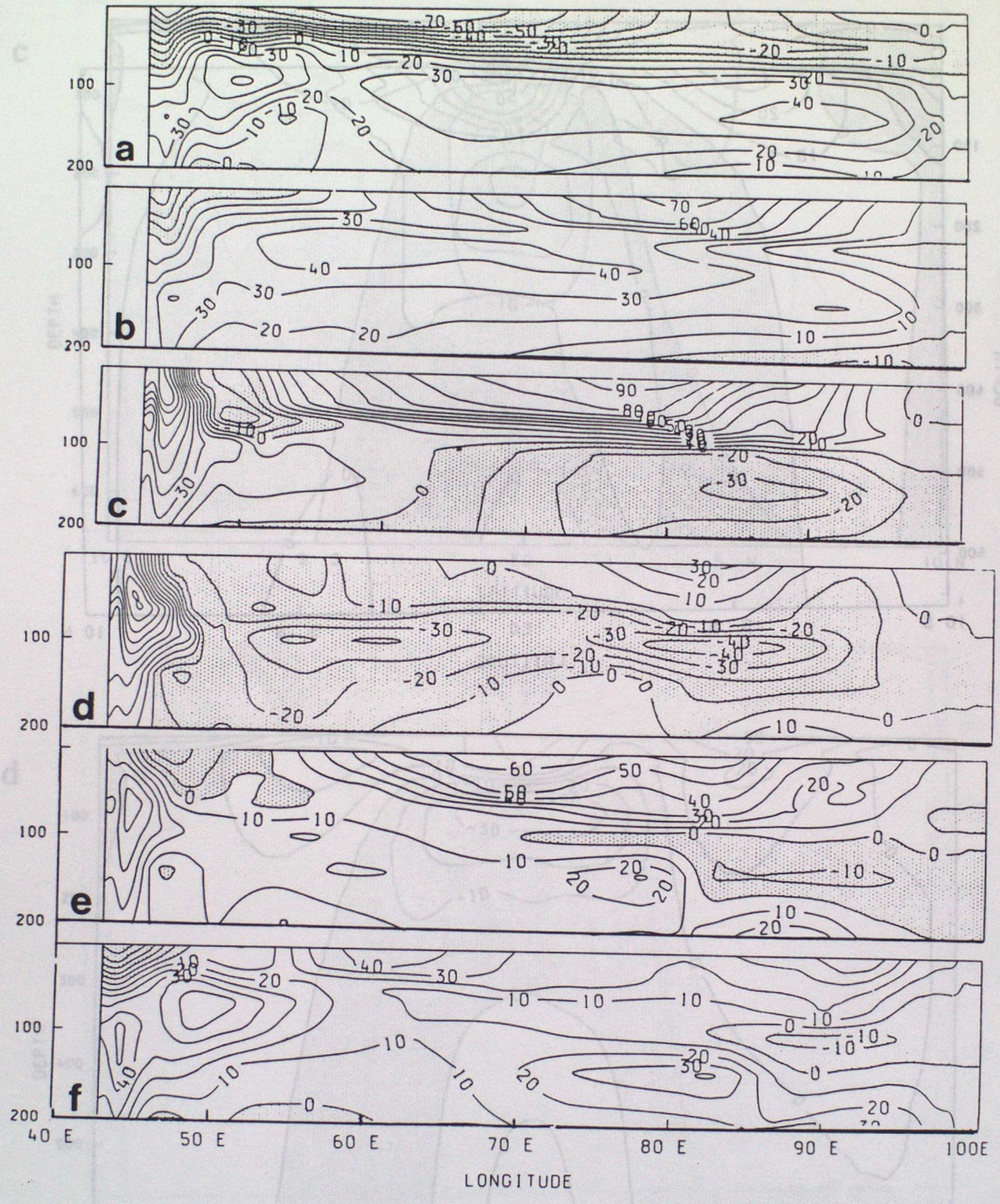

Fig. 8: Contours of zonal currents along the equator over the top 200 m at bimonthly intervals (westward velocities shaded). (a) February, (b) April, (c) June, (d) August, (e) October and (f) December. In the undercurrent depth band, strong eastward flow exists across most of the equatorial band for most of the year. The exception is in July and August, when the flow at this depth is westward over most longitudes and there are examples of reversed undercurrents, for example from 70°–90°E.

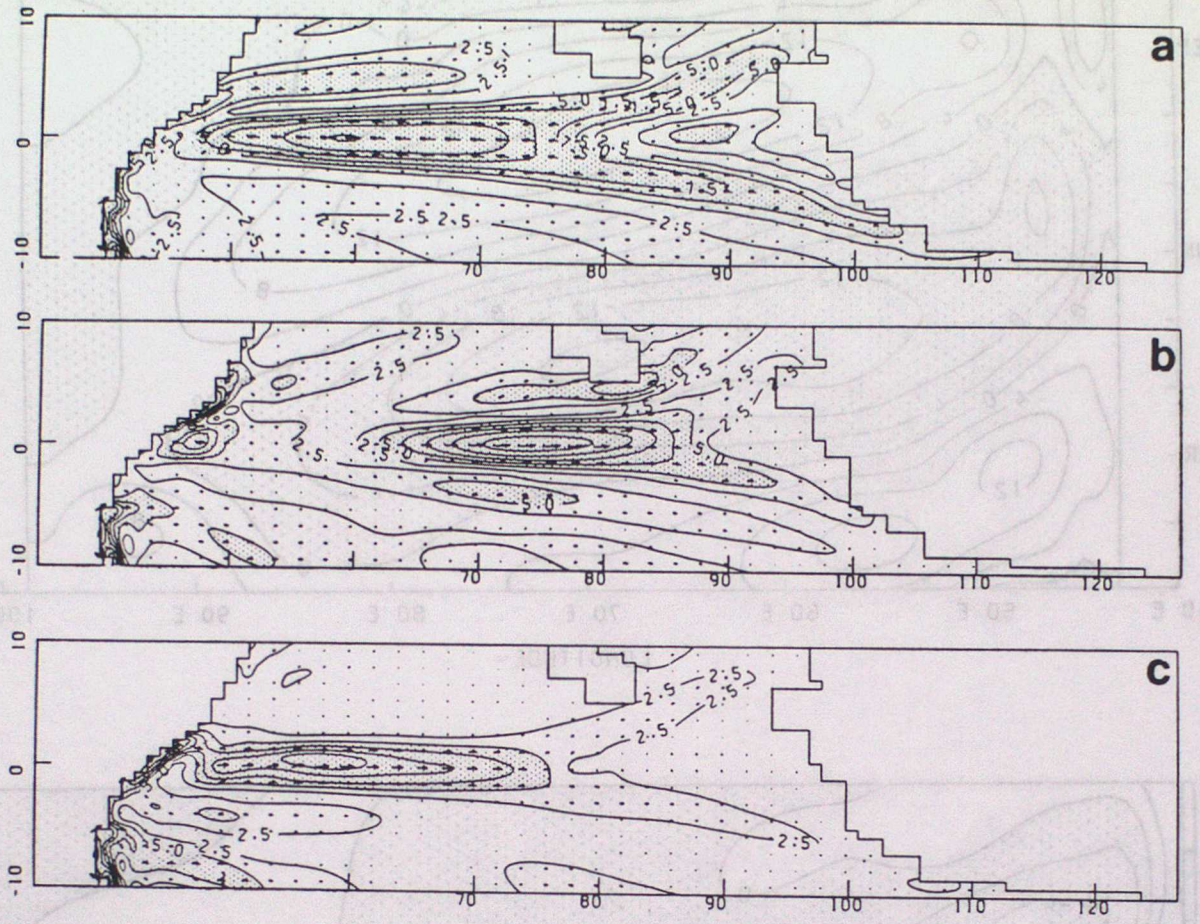

Fig. 9: Currents at 666 m for (a) May, (b) July and (c) September showing westward propagation, as expected from Fig. 5. The signal appears to be Rossby wave like and associated with the 2nd vertical mode. (Shading: >5 cms^{-1}.)

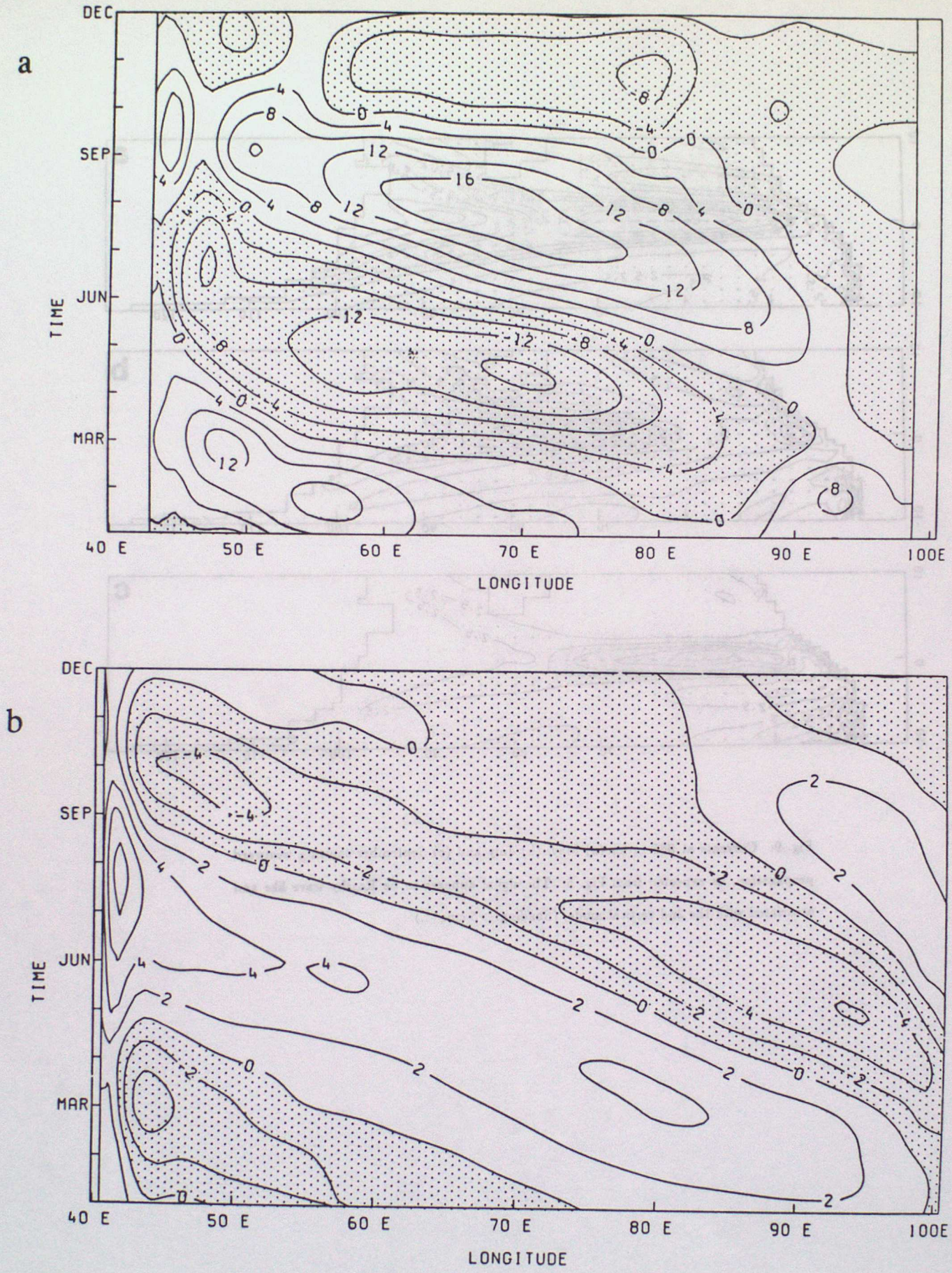

Fig. 10: Contours of zonal velocity at 666 m as a function of time (a) along the equator (b) along 5°S showing westward propagation at 2nd mode Rossby wave speeds. (Westward velocities shaded).

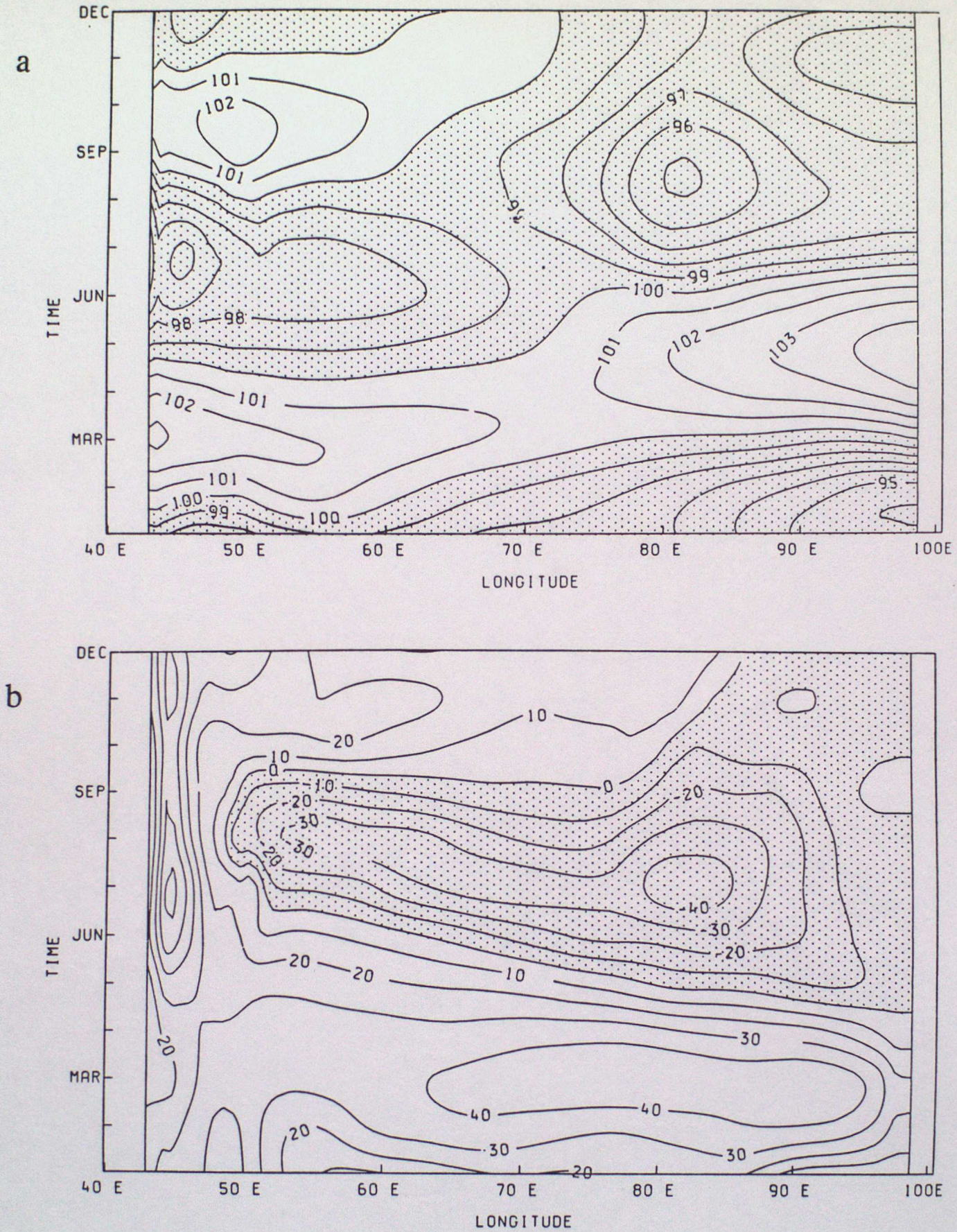

Fig. 11: Temporal evolution of (a) dynamic height at 113 m (in dynamic cm) relative to 800 m (values less than 100 dyn cm shaded) (b) zonal flow along the equator at 113 m (westward velocities shaded). The dynamic height is undercurrent favourable from September to March, when maximum eastward flow occurs. In April the dynamic height gradient reverses and the eastward flow weakens.

Appendix 1

Fig. A. Distribution of zonal velocity component (cm sec^{-1}) along the following sections. Eastward components are positive and westward components are negative. Shading indicates eastward flow.

II	53°E	Aug 2–10	1962
III	62°E	Aug 16–21	1962
IV	79°E	Aug 31–Sept 9	1962
V	89°E	Sept 11–21	1962
VI	85°E	Feb 19–26	1962
VII	61°E	Mar 7–12	1963
IX	92°E	Apr 20–25	1963
X	53°E	May 5–10	1963

From Taft and Knauss 1967.

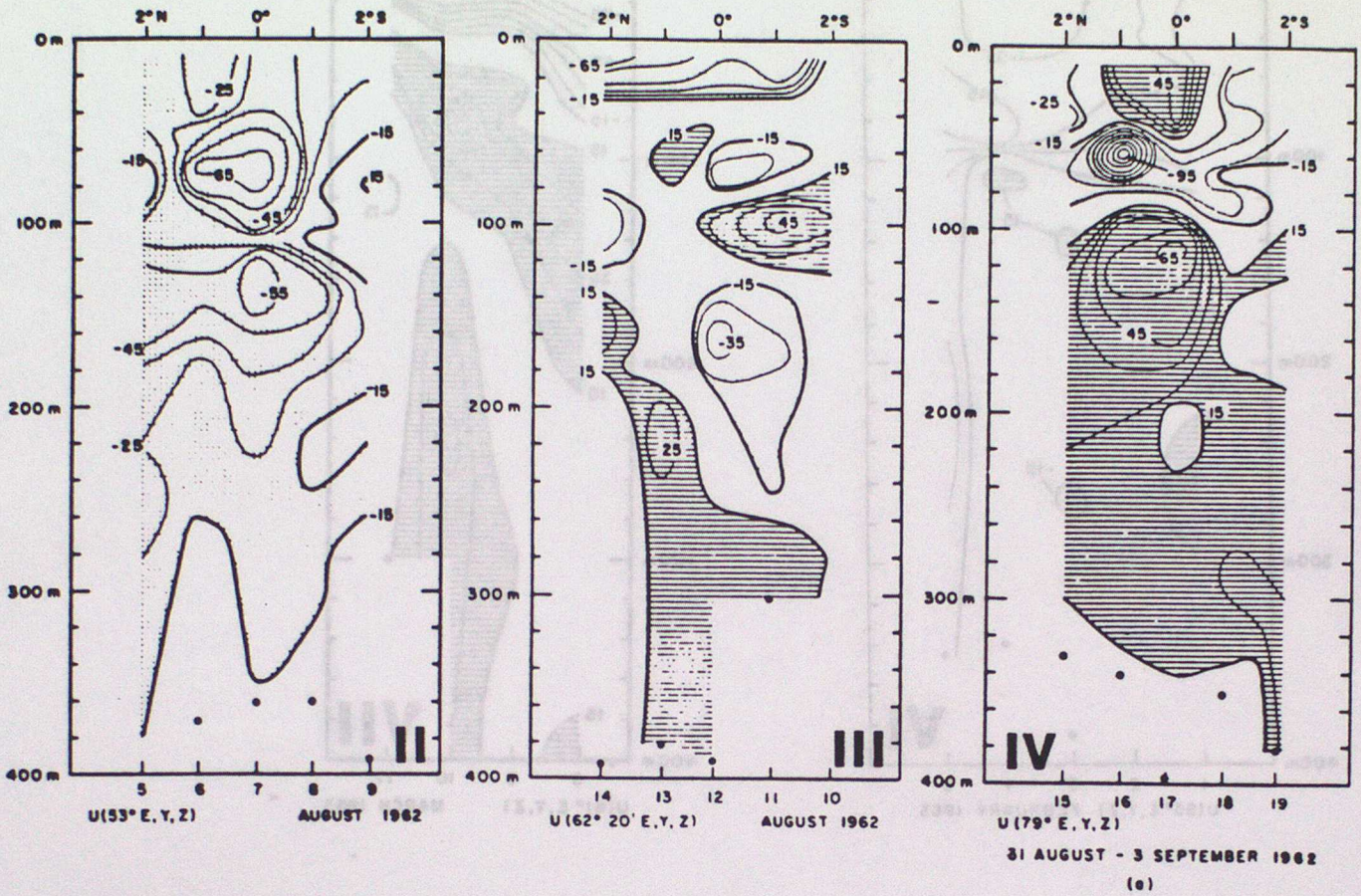
2°N
0°
2°S
0m
100m
200m
300m
400m
II
III
IV
U(53° E, Y, Z) AUGUST 1962
U(62° 20' E, Y, Z) AUGUST 1962
U(79° E, Y, Z)
31 AUGUST - 3 SEPTEMBER 1962
(a)

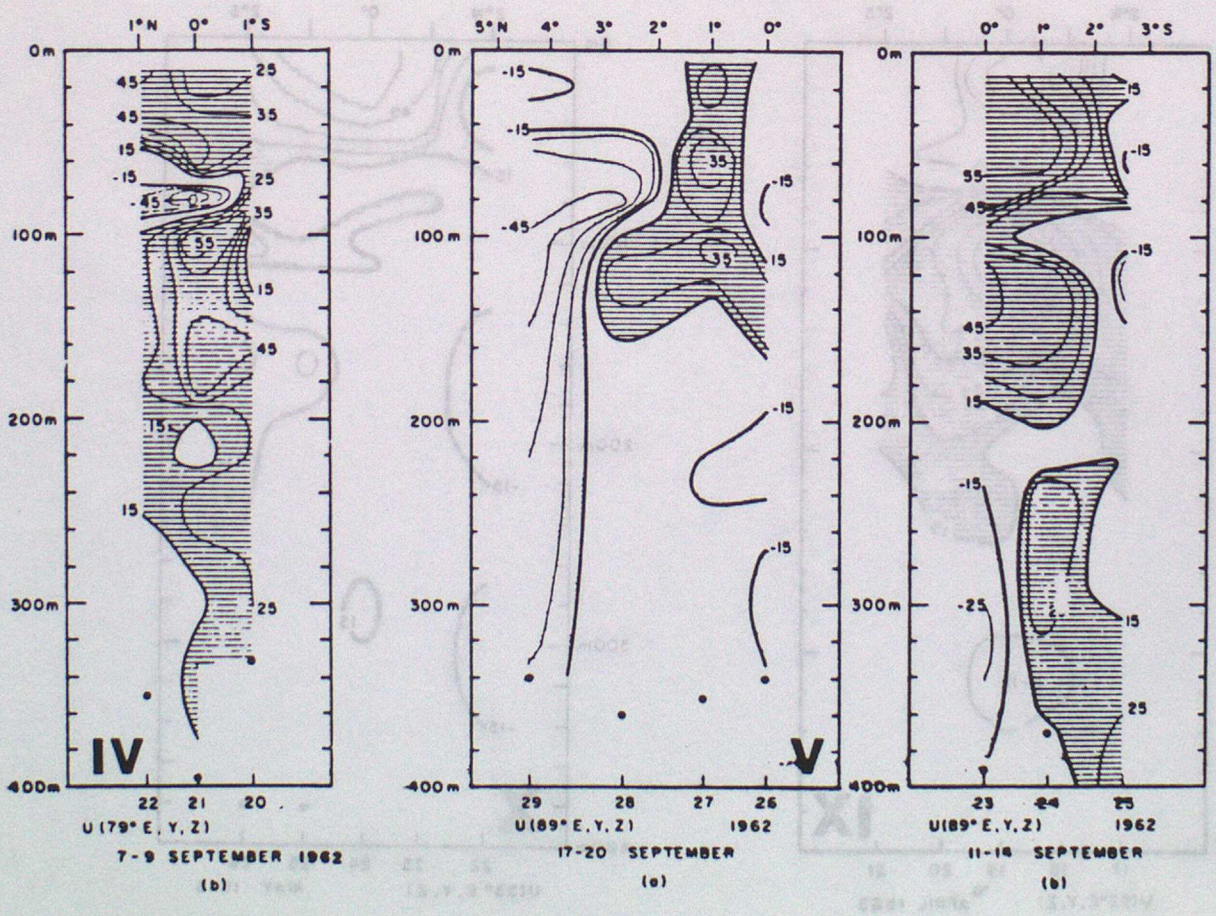
1°N
0°
1°S
5°N
4°
3°
2°
1°
0°
0°
1°
2°
3°S
0m
100m
200m
300m
400m
IV
V
U(79° E, Y, Z)
7-9 SEPTEMBER 1962
(b)
U(89° E, Y, Z) 1962
17-20 SEPTEMBER
(a)
U(89° E, Y, Z) 1962
11-14 SEPTEMBER
(b)

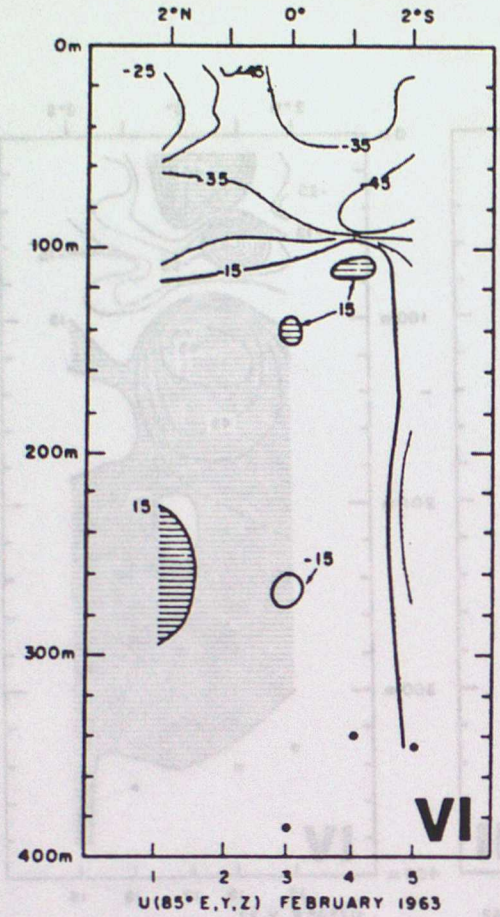
2°N
0°
2°S
0m
100m
200m
300m
400m
-25
-45
-35
-35
-45
-15
-15
15
-15
15
1
2
3
4
5
VI
U(85° E,Y,Z) FEBRUARY 1963

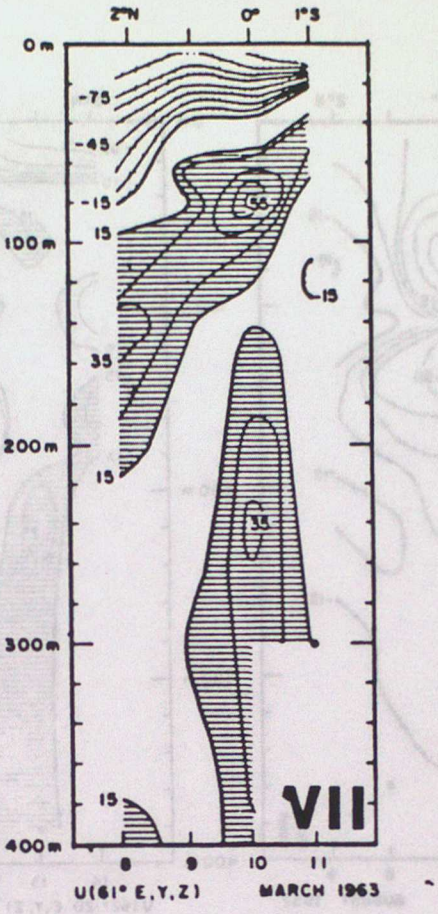
2°N
0°
1°S
0m
100m
200m
300m
400m
-75
-45
-15
15
55
15
35
15
35
15
8
9
10
11
VII
U(61° E,Y,Z) MARCH 1963

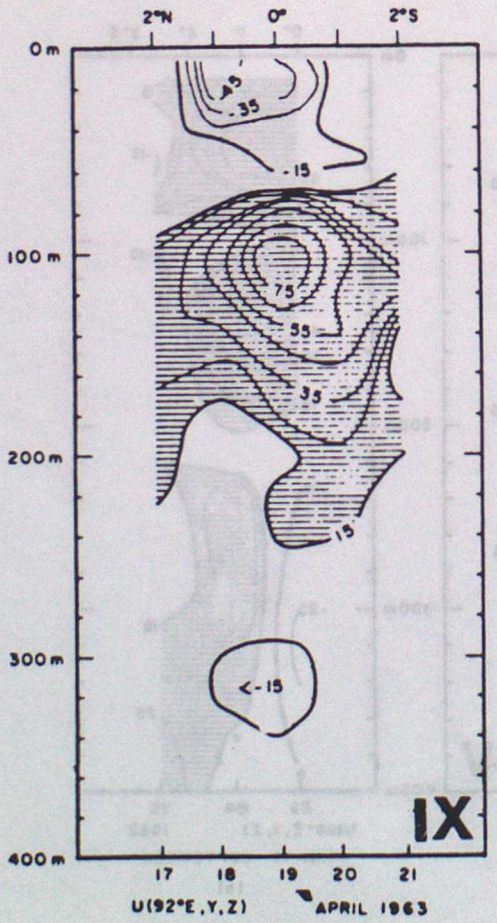
2°N
0°
2°S
0m
100 m
200m
300m
400m
-45
-35
-15
75
55
35
15
<-15
17
18
19
20
21
IX
U(92°E,Y,Z) APRIL 1963

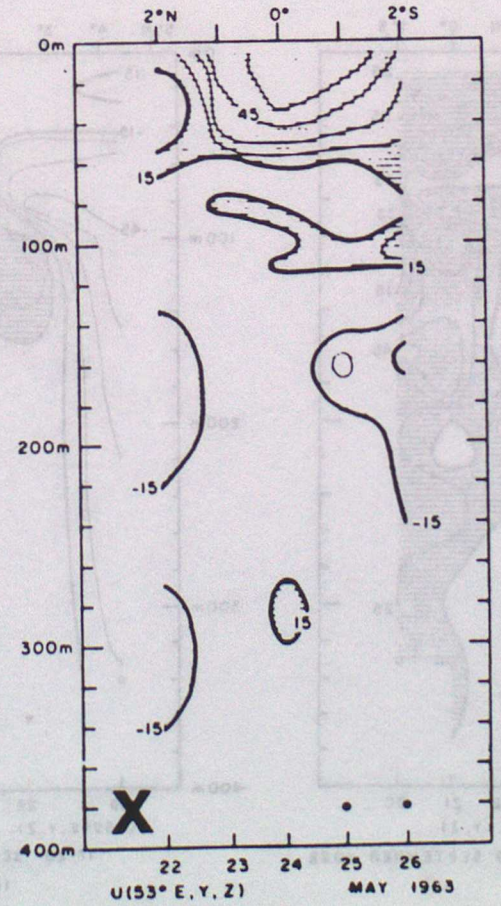
2°N
0°
2°S
0m
100m
200m
300m
400m
45
15
15
-15
-15
15
-15
22
23
24
25
26
X
U(53° E,Y,Z) MAY 1963

CLIMATE RESEARCH TECHNICAL NOTES

CRTN 1	Oct 1990	Estimates of the sensitivity of climate to vegetation changes using the Penman-Monteith equation. P R Rowntree
CRTN 2	Oct 1990	An ocean general circulation model of the Indian Ocean for hindcasting studies. D J Carrington
CRTN 3	Oct 1990	Simulation of the tropical diurnal cycle in a climate model. D P Rowell
CRTN 4	Oct 1990	Low frequency variability of the oceans. C K Folland, A Colman, D E Parker and A Bevan
CRTN 5	Dec 1990	A comparison of 11-level General Circulation Model Simulations with observations in the East Sahel. K Maskell
CRTN 6	Dec 1990	Climate Change Prediction. J F B Mitchell and Qing-cun Zeng
CRTN 7	Jan 1991	Deforestation of Amazonia - modelling the effects of albedo change. M F Mylne and P R Rowntree
CRTN 8	Jan 1991	The role of observations in climate prediction and research. D J Carson
CRTN 9	Mar 1991	The greenhouse effect and its likely consequences for climate change. D J Carson
CRTN 10	Apr 1991	Use of wind stresses from operational N.W.P. models to force an O.G.C.M. of the Indian Ocean. D J Carrington
CRTN 11	Jun 1991	A new daily Central England Temperature series, 1772-1991. D E Parker, T P Legg and C K Folland
CRTN 12	Jul 1991	Causes and predictability of Sahel rainfall variability. D P Rowell, C K Folland, K Maskell, J A Owen, M N Ward
CRTN 13	Jul 1991	Modelling changes in climate due to enhanced CO_2, the role of atmospheric dynamics, cloud and moisture. C A Senior, J F B Mitchell, H Le Treut and Z-X Li

CLIMATE RESEARCH TECHNICAL NOTES

CRTN 14	Sep 1991	Sea temperature bucket models used to correct historical SST data in the Meteorological Office. C K Folland
CRTN 15	Aug 1991	Modelling climate change, and some potential effects on agriculture in the U.K. P R Rowntree, B A Callander and J Cochrane
CRTN 16	Aug 1991	The Boreal Forests and Climate G Thomas and P R Rowntree
CRTN 17	Aug 1991	Development of a Stratosphere-Troposphere Data Assimilation System. R Swinbank.
CRTN 18	Sep 1991	A study of asynchronous coupling using a simple climate model. M K Davey.
CRTN 19	Sep 1991	The Oceanic Carbon Cycle. N K Taylor
CRTN 20	Nov 1991	Worldwide ocean-atmosphere surface fields in Sahel wet and dry years using provisionally corrected surface wind data. M N Ward
CRTN 21	Dec 1991	Coupled tropical ocean global atmosphere models at the UKMO. M K Davey, C Gordon, S Ineson and S Lawrence
CRTN 22	Dec 1991	Empirical parameterisation of tropical ocean-atmosphere coupling. M Allen, M K Davey, D L T Anderson and P D Killworth
CRTN 23	Feb 1992	The temporal evolution of Equatorial Currents in the Indian Ocean